AGU PUBLICATIONS

Water Resources Research

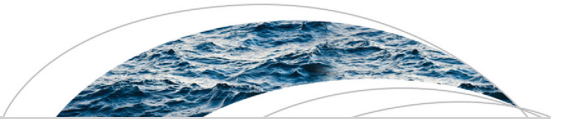

RESEARCH ARTICLE

10.1002/2015WR018046

Key Points:
- Drainage relative permeability is measured for CO_2-brine and N_2-water and scaled by capillary number
- The CO_2-brine system is very sensitive to capillary pressure heterogeneity
- Reservoir characterization should be performed on heterogeneous core samples

Correspondence to:
C. A. Reynolds,
catriona.reynolds11@imperial.ac.uk

Citation:
Reynolds, C. A., and S. Krevor (2015), Characterizing flow behavior for gas injection: Relative permeability of CO_2-brine and N_2-water in heterogeneous rocks, *Water Resour. Res.*, *51*, 9464–9489, doi:10.1002/2015WR018046.

Received 1 SEP 2015
Accepted 13 NOV 2015
Accepted article online 18 NOV 2015
Published online 12 DEC 2015

Characterizing flow behavior for gas injection: Relative permeability of CO_2-brine and N_2-water in heterogeneous rocks

C. A. Reynolds[1] and S. Krevor[1]

[1]Qatar Carbonates and Carbon Storage Research Centre, Department of Earth Science and Engineering, Imperial College London, London, UK

Abstract We provide a comprehensive experimental study of steady state, drainage relative permeability curves with CO_2-brine and N_2-deionized water, on a single Bentheimer sandstone core with a simple two-layer heterogeneity. We demonstrate that, if measured in the viscous limit, relative permeability is invariant with changing reservoir conditions, and is consistent with the continuum-scale multiphase flow theory for water wet systems. Furthermore, we show that under capillary limited conditions, the CO_2-brine system is very sensitive to heterogeneity in capillary pressure, and by performing core floods under capillary limited conditions, we produce effective relative permeability curves that are flow rate and fluid parameter dependent. We suggest that the major uncertainty in past observations of CO_2-brine relative permeability curves is due to the interaction of CO_2 flow with pore space heterogeneity under capillary limited conditions and is not due to the effects of changing reservoir conditions. We show that the appropriate conditions for measuring intrinsic or effective relative permeability curves can be selected simply by scaling the driving force for flow by a quantification of capillary heterogeneity. Measuring one or two effective curves on a core with capillary heterogeneity that is representative of the reservoir will be sufficient for reservoir simulation.

1. Introduction

Relative permeability curves are a fundamental input to reservoir models which provide the only way to predict the subsurface flow and trapping of CO_2. There is still much controversy surrounding the measurement of CO_2-brine relative permeability curves. What parameters impact relative permeability (rock heterogeneity, fluid properties such as viscosity and interfacial tension etc.)? Do the relative permeability curves measured on small samples in the lab provide a sufficient basis from which to predict fluid migration over a reservoir? How do we perform such measurements successfully given the difficulties of using a low-viscosity fluid like supercritical CO_2, the corrosive nature of CO_2-brine mixtures and the potential for mass transfer of CO_2 out of the experimental system.

There is now a significant body of published drainage and imbibition relative permeability curves for the CO_2-brine system in sandstones (see *Benson et al.* [2013] for a recent compilation). Where systematic studies have been made, most rely on using dimensionless groups such as the capillary number [e.g., *Bachu and Bennion*, 2008] to investigate the response of CO_2-brine relative permeability to changing reservoir conditions. Else, measurements are made on separate cores at a single specific reservoir condition and as a result few general conclusions about the behavior of the CO_2-brine system have been drawn.

Many unexpected field-scale observations of CO_2 injectivity, early breakthrough, and plume shape may also be conceivably caused by a misunderstanding of CO_2-brine relative permeability. *Rogers and Grigg* [2000] suggest abnormal changes in injectivity after CO_2 injection may be the result of a poor understanding of the impact of geological heterogeneity on relative permeability, especially in reservoirs where there may be cross flow between units. *Cavanagh* [2013] and *Cavanagh and Nazarian* [2014] found that the plume shape observed at the Sleipner injection site can only be matched using capillary flow simulations, not Darcy or viscous flow. The early breakthrough of CO_2 observed at the Frio pilot injection site by *Hovorka et al.* [2006] is also likely to be a manifestation of capillary limited, rather than viscous limited flow, under which conditions rock heterogeneity will have a greater effect on the CO_2 pathway.

In this work, we explore the impact of reservoir conditions and capillary heterogeneity on the relative permeability of the CO_2-brine system. Pressure, temperature, and brine salinity have been varied across a wide range of conditions representative of CO_2 storage targets worldwide, while performing tests in a single Bentheimer sandstone core with a simple two-layer heterogeneity. We measure relative permeability using the steady state method, under conditions of constant total flow rate or constant fractional flow in order to investigate how the balance of capillary and viscous forces control the spatial distribution of CO_2 in the core.

2. Observations of the Response of CO_2-Brine Flow Properties to Reservoir Conditions

Past work characterizing relative permeability has resulted in suggestions that the CO_2-brine system is particularly sensitive to variations in reservoir conditions, through the impacts of these conditions on fluid and fluid-rock properties, such as interfacial tension, viscosity, and wetting.

The wetting state of the CO_2-brine system in sandstone rocks has been suggested to be less water-wet than decane-brine by *Berg et al*. [2013] using unsteady state observations of drainage and not water-wet by *Levine et al*. [2014] through a characterization of the drainage endpoint relative permeability. However, *Pentland et al*. [2011], *Pini et al*. [2012], and *Al-Menhali et al*. [2015] all found positive entry pressures and an invariance with reservoir conditions of the drainage capillary pressure characteristic curve, suggesting the system is water-wet during drainage. The significant hysteresis between drainage and imbibition processes observed by *Akbarabadi and Piri* [2013], *Ruprecht et al*. [2014], and *Al-Menhali et al*. [2015] and the invariance of the initial-residual trapping relationship across a range of reservoir conditions observed by *Niu et al*. [2015] and *Krevor et al*. [2015] show the system is also water-wet during imbibition. Observations of relative permeability by *Krevor et al*. [2012], *Akbarabadi and Piri* [2013], *Pini and Benson* [2013], and *Manceau et al*. [2015] all show that reported observations of a low endpoint relative permeability to CO_2 are not a result of a weakened wetting, but due the limitations of the experimental apparatus used, which mean capillary pressures approaching the endpoint cannot be obtained using the conventional steady state protocol.

Bachu and Bennion [2008] report that relative permeability curves are sensitive to variation in either interfacial tension or viscosity with changing pressure. However, *Egermann et al*. [2006] found that drainage displacements in CO_2-brine systems could be modeled using relative permeability data derived from N_2-water displacements so long as the variation in thermophysical properties were taken into account.

In this study, we perform a comprehensive and systematic suite of drainage relative permeability measurements in order to confirm which, if any, fluid parameters affect CO_2-brine relative permeability.

3. The Impact of Rock Heterogeneity on Flow Properties

Perrin and Benson [2010], *Shi et al*. [2011], *Pini et al*. [2012], *Wei et al*. [2014], and *Zhang et al*. [2014] have demonstrated the prevalent impact that small-scale rock heterogeneity has for CO_2-brine systems through observations of the distribution of CO_2 in rocks during core flood experiments in nominally homogeneous cores. *Krause et al*. [2013] and *Kong et al*. [2015] have shown that it is heterogeneity in the capillary pressure characteristics of the rocks that are primarily responsible for this effect using detailed numerical models of core floods, while *Kuo and Benson* [2013] and *Krause and Benson* [2015] show that this can result in an apparent dependence of the flow properties on reservoir conditions and fluid velocities.

This suggests that the observed sensitivity of CO_2-brine relative permeability to reservoir conditions could be the manifestation of an effect that rock heterogeneity has in this system. This also raises broader questions about the scaling that should be applied to the measurement of flow properties in the laboratory, and the guidance for the use of these measurements in field-scale simulation. Evaluating the impact of rock heterogeneity on flow properties, including the interplay with fluid thermophysical properties and reservoir conditions in this system, is one of the key aims of this work.

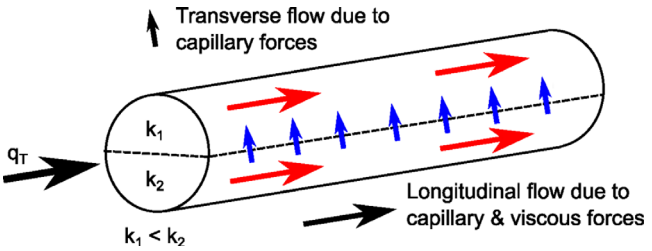

Figure 1. Transverse and longitudinal flow in a core with a simple layered heterogeneity in absolute permeability, *k*.

4. Scaling Relative Permeability in Heterogeneous Rocks Using a Dimensionless Capillary Number

The relative importance of capillary-driven flow to viscously-driven flow—and by extension, the relative importance of capillary heterogeneity to permeability heterogeneity—is generally characterized through a dimensionless capillary number, which can be defined in various ways depending on the application.

Scaling analysis has been applied to multiphase flow in geologic systems to identify the varied roles of fluid and rock properties at a range of length scales by *Shook et al*. [1992] and *Rapoport* [1955] and has been extended to characterize the impacts of rock heterogeneity by *Yokoyama and Lake* [1981], *Zhou et al*. [1997], and *Jonoud and Jackson* [2008], where heterogeneity is represented through changes in both absolute permeability and capillary pressure characteristic curves.

For systems with heterogeneity, a capillary number that compares viscous fluid velocities in a principal direction (e.g., along the length of a rock core) to capillary-driven flow transverse to this is a key measure of the importance of capillary and permeability heterogeneity in the system [*Jonoud and Jackson*, 2008]. This is sometimes referred to as a *transverse capillary number*, $N_{c,T}$.

A commonly used transverse capillary number is defined by *Yokoyama and Lake* [1981] and *Zhou et al*. [1997] as:

$$N_{c,T} = \frac{H^2 q \mu_o}{L p_c^* k_T}, \tag{1}$$

where L and H (m) are length scales in the principal and transverse directions (e.g., in a rock core, along the axis, and the diameter, respectively), p_c^* (Pa) is a characteristic capillary pressure (entry or modal capillary pressure), k_T (m^2) is the permeability in the transverse direction, q ($m\ s^{-1}$) is the total fluid velocity in the principal direction, and μ_o (Pa s) is the viscosity of the nonwetting phase.

Consider a drainage displacement of water by CO_2 in a simple two-layered core (Figure 1), when $N_{c,T} \gg 1$, viscous forces dominate the flow resulting in both sides of the core being invaded equally by CO_2 [*Zhou et al*., 1997]. If $N_{c,T} \ll 1$, capillary forces drive fluid flow in the transverse direction resulting in the imbibition of water into the low-permeability layer, so that most of the CO_2 invades the high-permeability layer. This capillary redistribution is termed "cross flow." We use a rock core with the same two-layer heterogeneity to investigate the viscous-capillary force balance during CO_2 and N_2 injection in this study.

Virnovsky et al. [2004] define a capillary number,

$$N_c = \frac{H}{|\Delta P_c(f_w)|} \frac{\Delta P}{L}, \tag{2}$$

where the contribution from capillarity is given by the magnitude of a characteristic difference in capillary pressure, $|\Delta P_c|$ and the viscous component is given by the pressure drop, ΔP. The benefit of this formulation is that it allows the viscous pressure drop measured during an experiment to be compared directly with the measured capillary heterogeneity for the core sample and no specific directionality for the capillary contrast needs to be defined. Equation (2) also acknowledges that the importance of capillary heterogeneity will vary as a function of fractional flow. We use this formulation to characterize the core floods in this study.

Equations (1) and (2) give a measure of the relative importance of capillary and viscous forces in distributing fluids, depending on the spatial scale of inspection, the capillary properties of the rock (capillary pressure and absolute permeability), the viscous fluid flow velocity, and the displacing fluid viscosity. The larger the numbers, the closer the system is to a *viscous limit*, where saturation is determined purely by the distribution of the absolute permeability in the domain. The saturation is homogenous across layers with different

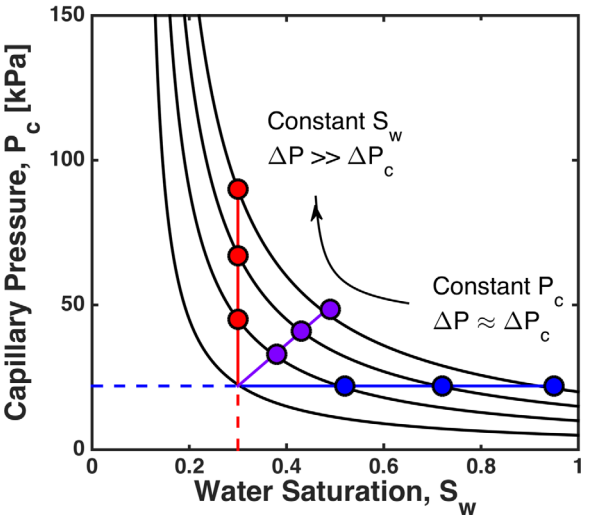

Figure 2. The impact of capillary heterogeneity on the saturation distribution as the flow domain transitions from a capillary (constant P_c) to viscous limiting case (constant S_w).

capillary properties if the system is characterized by a single relative permeability curve (Figure 2, blue line). The smaller the number, the closer the system is to the *capillary limit*, where capillary pressure is constant and variation in saturation is governed by heterogeneity in the capillary pressure characteristic curves (Figure 2, red line). Intermediate behavior is observed over the transition between these limits (Figure 2, purple line).

Figure 3 shows a compilation of capillary numbers, N_c, calculated for steady state drainage CO_2-brine relative permeability data measured on sandstones and carbonates at various fluid and flow conditions from *Bennion and Bachu* [2005, 2006a, 2006b], *Bachu and Bennion* [2008], *Bennion and Bachu* [2008], *Perrin and Benson* [2010], *Krevor et al*. [2012], *Akbarabadi and Piri* [2013], *Kogure et al*. [2013], *Krause et al*. [2013], *Pini and Benson* [2013], *Zhang et al*. [2013], *Ruprecht et al*. [2014], and *Manceau et al*. [2015]. Where possible, the reported values of ΔP are used, else the pressure drop is calculated from the reported relative permeability data (see equation (4) in section 6.1). For data measured on Berea sandstone, a constant $|\Delta P_c|$ of 5000 Pa is used, taken from *Pini et al*. [2012], else the reported capillary entry pressure or $|\Delta P_c|$ for the rock sample is used. For the experiments in this study, the measured $|\Delta P_c(f_w)|$ is used. Further discussion of this calculation is provided in section 10.

The majority of the data in Figure 3 is measured under capillary-dominated conditions, which we will argue in this paper, is the reason some authors find a dependence of CO_2-brine relative permeability on reservoir conditions.

Although these capillary numbers qualitatively describe scaling in heterogeneous systems, *Pickup and Stephen* [2000] point out they cannot be used to reliably predict the precise number where a flow system is dominated by capillary or viscous (permeability) heterogeneity. *Virnovsky et al*. [2004] find that the transition is dependent on the specific heterogeneity, i.e., not just characteristic capillary pressure differences but also the spatial pattern of the heterogeneity itself. For example, a rock composed of horizontal layers with alternating high and low absolute permeability may have the same effective permeability as a rock with a low-permeability matrix and irregularly distributed high-permeability streaks, but the transition from capillary to viscous dominated flow will not necessarily occur at the same capillary number. However, transitions from a capillary limit to a viscous limit to generally occur for a number of system types in the range $0.1 < N_c < 100$. For the experimental

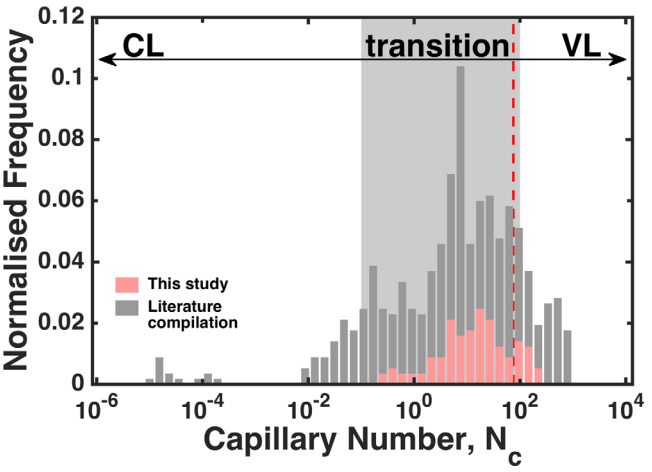

Figure 3. Histogram of calculated N_c for every steady state relative permeability data point in this study and from a literature compilation [*Akbarabadi and Piri*, 2013; *Bennion and Bachu*, 2005, 2006a, 2006b; *Bachu and Bennion*, 2008; *Bennion and Bachu*, 2008; *Perrin and Benson*, 2010; *Krevor et al*., 2012; *Kogure et al*., 2013; *Krause et al*., 2013; *Pini and Benson*, 2013; *Zhang et al*., 2013; *Ruprecht et al*., 2014; *Manceau et al*., 2015]. Transition from capillary limit (CL) to viscous limit (VL) is expected in the range $10^{-1} < N_c < 10^3$ (grey bar) *Virnovsky et al*. [2004] and occurs at $N_c \approx 75$ (red dashed line) for the data set in this study (see section 10).

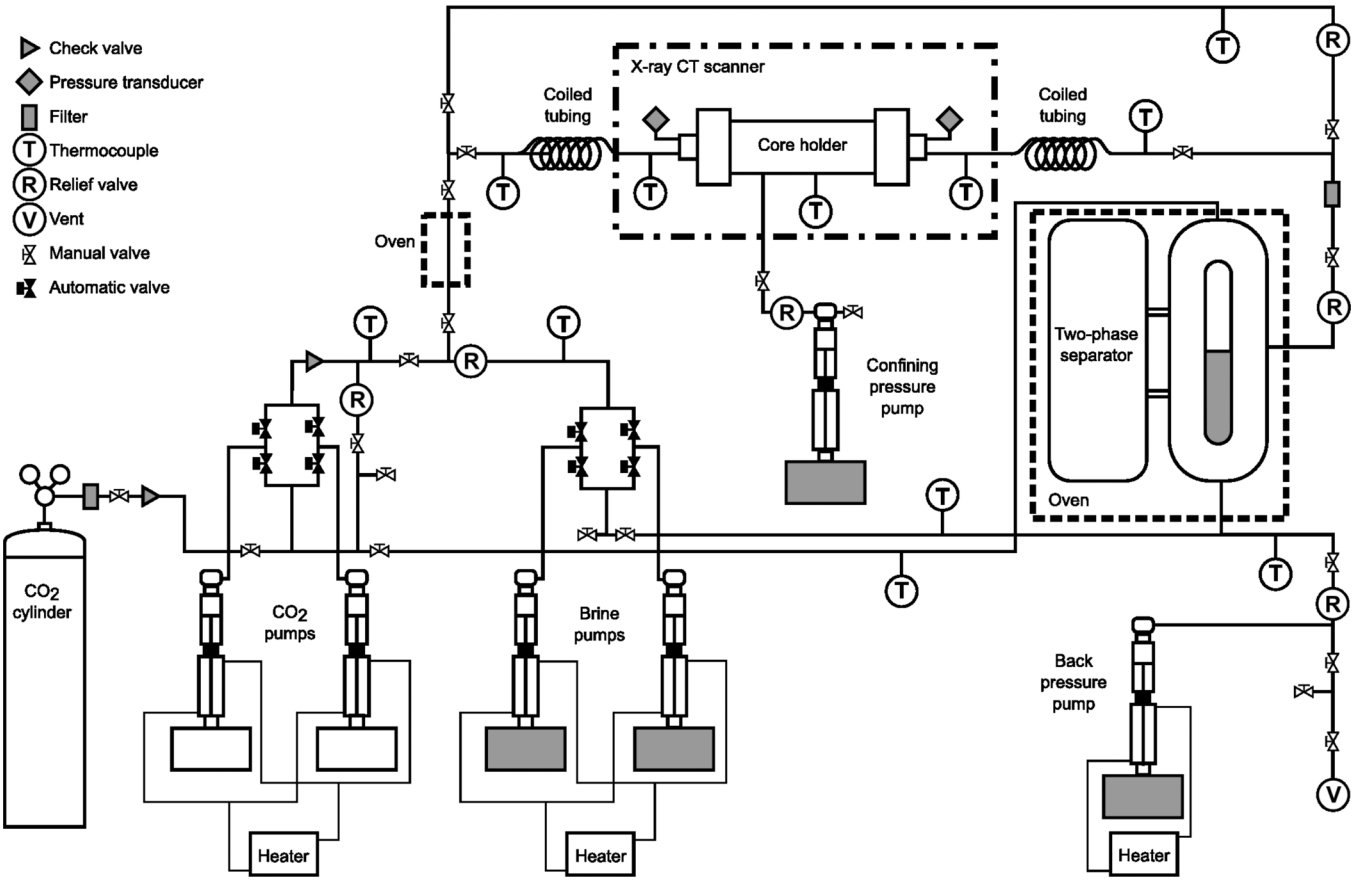

Figure 4. High-pressure, high-temperature flow loop used for steady state relative permeability experiments.

results presented in this work, we find a transition at around $N_c \approx 10–75$, depending on fluid saturation (illustrated in Figure 3).

From equation (1), it is clear that viscous forces dominate at larger length scales, higher flow velocities, and higher fluid viscosities. Using $q = 1$ m/d, $H/L = 0.2$, $p_c^* = 10$ kPa, $k_T = 10$ mD, and $\mu_{CO_2} = 2.5 \times 10^{-5}$ Pa s, capillary and viscous forces are approximately equal at length scales of 10 m and capillary forces become significant at less than 1 m. This is the length scale at which reservoir flow properties are characterized in the laboratory. Typical pressure drops during core-scale experiments range from 10 to 500 kPa, which means that for $H/L = 0.2$ and $\Delta P_c = 10$ kPa, equation (2) gives capillary numbers in the range of $0.2 < N_c < 10$, the range at which the transition from capillary to viscous dominated flow conditions is predicted to occur by *Virnovsky et al*. [2004]. An evaluation of the potential for an impact of capillary heterogeneity on flow during the characterization of a core is thus of key importance for understating the appropriate steps to take for both the design of the observation test and in the subsequent use of the derived flow property in reservoir simulation.

If capillary forces dominate the fluid distribution at the scale at which relative permeability is measured, this will have an effect on the derived flow functions used to model reservoir-scale fluid flow. This has been confirmed experimentally for hydrocarbon systems by *Honarpour et al*. [1995] and through modeling for the CO_2-brine system by *Krause and Benson* [2015]. *Corbett et al*. [1992] and *Ringrose et al*. [1993] suggest the "geo-pseudo" approach to the use of constitutive flow relationships, where core-scale relative permeability curves must be measured on each separate stratal element that makes up a heterogeneous rock and then averaged, before using the scale-up procedure normally used to derive pseudorelative permeability curves [e.g., *Kyte and Berry*, 1975]. This was acknowledged as an "unsatisfying aspect of the method." We will argue in this work that pseudo or effective flow functions, measured at low capillary number, can and should be directly performed on the heterogeneous rock cores themselves, if the appropriate scaling is used to represent the conditions prevalent in the reservoir.

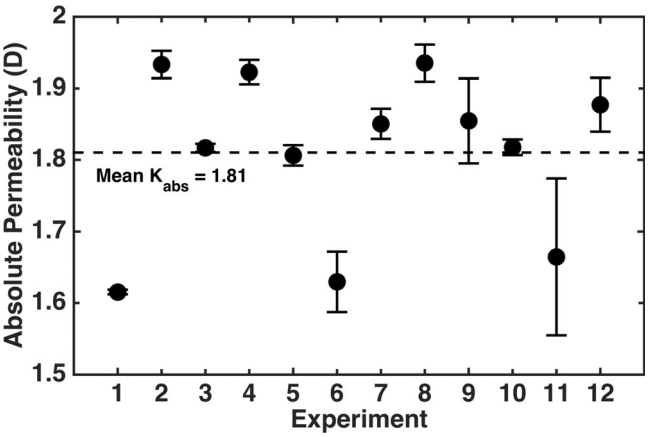

Figure 5. Absolute permeability to brine or deionized water measured at experimental conditions, at the beginning of each experiment.

5. Objectives of This Study

In this work, we will draw on the above mentioned theoretical framework and our own observations in a number of CO_2-brine and N_2-brine core flood experiments to show that the vast number of reported observations of relative permeability for CO_2-brine systems were made in a system far from the viscous limit where the fractional flow interpretation is valid for the derivation of relative permeability. When measured in the viscous limit, the true, *intrinsic* relative permeability of the rock is measured, which is invariant under changing reservoir conditions and the distribution of the nonwetting phase in the pore space is not controlled by capillary pressure heterogeneity. Under capillary limited conditions, an *effective* relative permeability is measured, which appears flow rate and fluid parameter dependent through the impact of these properties on the capillary redistribution of the nonwetting phase and is strongly controlled by capillary pressure heterogeneity in the core. We also provide guidance as to how to fully characterize the flow behavior expected in a heterogeneous reservoir by performing a minimum number of relative permeability measurements which capture the impact of the dominant heterogeneity at the range of capillary number conditions predicted.

6. Experimental Method

6.1. Steady State Relative Permeability

The multiphase extension to Darcy's is given by *Muskat and Meres* [1936],

$$v_{ix} = -K\frac{k_{ri}}{\mu_i}\frac{\partial \Phi_i}{\partial x}, \tag{3}$$

and relates v_{ix}, the volumetric flux per unit area of a fluid phase i in the x direction, to K, the absolute permeability of the medium, $k_{r,i}$ and μ_i, the relative permeability and viscosity of i, and $\partial\Phi_i/\partial x$, the potential energy gradient of i, where i is CO_2 or brine and x is the principal flow direction. We assume (1) the flow can be approximated as one dimensional in x, in a homogeneous and isotropic medium, (2) the fluid phases are immiscible and incompressible, (3) transport under gravity and capillary forces is negligible, and (4) the fluid distribution at the inlet is uniform [*Pope*, 1980]. Under these conditions, equation (3) can be simplified to:

$$q_i = -\frac{Akk_{r,i}(S_i)}{\mu_i}\frac{\Delta P}{L}, \tag{4}$$

and the relative permeability at steady state saturation $k_{r,i}(S_i)$ calculated for a constant pressure drop, ΔP, and continuous injection at velocity q_i into a core with length L and cross-sectional area A.

Table 1. Experiment Type[a]

Experiment	NW Phase	Flow Parameter Held Constant	Parameter Controlling ΔP
1–7	CO_2	$q_T = 20$ mL/min	μ_{CO_2}
8		$q_T = 20$ mL/min	
9	N_2	$q_T = 7$ mL/min	q_T
10		$q_T = 40$ mL/min	
11	N_2	$f_{N_2} = 0.5$	q_T
12		$f_{N_2} = 0.993$	

[a]Total flow rate, q_T, and nonwetting phase viscosity, μ_{CO_2} are used to control the viscous pressure drop, ΔP, and thus viscous-capillary force balance during a core flood.

Table 2. Experimental Conditions and Fluid Parameters for CO_2-Brine and N_2-Water Core Floods

Experiment	NW Phase	T (°C)	P (MPa)	S[a] (mol/kg)	IFT[b] (mN/m)	M	D	μ_{nw}[c] (μPa s)	μ_w[d] (μPa s)	ρ_{nw}[d] (kg/m^3)	ρ_w[e] (kg/m^3)
1	CO_2	38	20.7	0	29	0.12	1.17	81.8	679.6	856.4	1005.6
2	CO_2	91	10.3	0	37	0.07	4.59	22.1	314.0	209.9	963.4
3	CO_2	42	13.5	3	37	0.07	1.47	61.3	868.2	736.1	1078.7
4	CO_2	65	10.5	3	41	0.04	3.64	24.3	608.8	292.0	1064.0
5	CO_2	40	10.7	0	34	0.08	1.49	52.7	653.9	671.7	1003.5
6	CO_2	85	13.3	0	34	0.08	2.94	27.0	337.3	329.7	968.7
7	CO_2	41	12.1	5	41	0.05	1.59	57.9	1120.6	711.2	1132.1
8–12	N_2	50	15.5	0	62	0.04	6.43	22.1	549.9	155.0	996.5

[a]NaCl brine.
[b]*Li et al.* [2012].
[c]http://webbook.nist.gov/chemistry/.
[d]*Kestin et al.* [1981].
[e]*Phillips et al.* [1981].

Drainage relative permeability is measured by coinjecting CO_2 and brine into an initially brine-saturated core. The fractional flow of CO_2, $f_{CO_2} = q_{CO_2}/q_T$, is increased in a stepwise manner from 0 to near 1. After each change in f_{CO_2}, the fluids are allowed to reach steady state, i.e., when there is a constant saturation profile and a constant pressure drop (ΔP) along the length of the core. The relative permeability to each fluid at the core-averaged saturation ($k_{r,i}(S_i)$) can then be calculated using equation (4). The f_{CO_2} is then increased, maintaining a constant q_T and the system allowed to reach steady state again.

6.2. Description of Flow Loop

Core floods are conducted in a high-pressure, high-temperature, corrosion-resistant flow loop (Figure 4). Dual CO_2 and brine pumps (Teledyne Isco, model 500D) are used to cocirculate fluids. Automatic valve packages control the flow and refill of the pumps so that CO_2 and brine may be continuously circulated for several days. Fluids are circulated through a core holder (Phoenix Instruments, custom) in a horizontal orientation, to a two-phase separator (Vinci Technologies, custom) from which they are returned to the pumps. A back pressure pump (Teledyne Isco, model 500D) on the outlet side of the core is used to maintain the system pressure and a confining pump (Teledyne Isco, model 100DX) applies an overburden of 3–5 MPa over the experimental pressure to the core. All flow lines and pumps are constructed from a corrosion resistant alloy (Hastelloy). The core holder is constructed from aluminum, which is transparent to X-rays. Pressure is measured at the inlet and outlet face of the core using high-accuracy pressure transducers (Digiquartz Intelligent transmitter, Model 410K-HT-101, oil-filled). All flow lines, pumps, the separator, and core holder are heated using heating lines, ovens, or heating baths where appropriate and the temperature is continuously monitored at in excess of 20 positions around the flow loop to ensure the experimental temperature is maintained throughout the experiment. Pump pressures and volumes, and

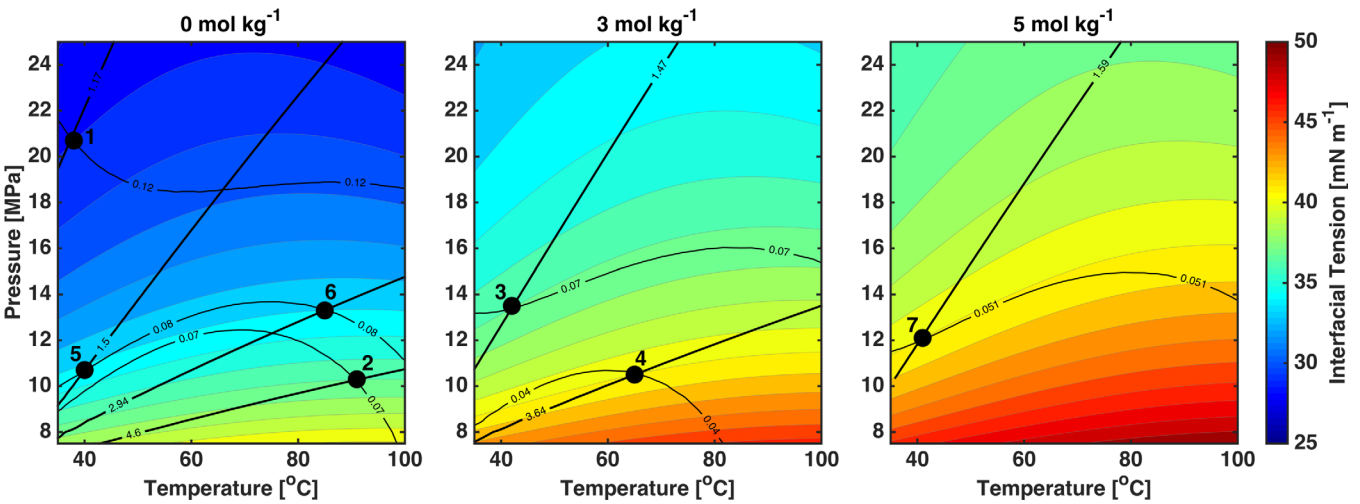

Figure 6. Conditions of CO_2-brine core floods. Interfacial tension is calculated for three NaCl brine molalities and plotted as a function of pressure and temperature [*Li et al.*, 2012]. Bold black lines show constant density ratio (1.17–3.64) and thin black lines show constant viscosity contrast (0.04–0.12). Numbered dots correspond to conditions in Table 2.

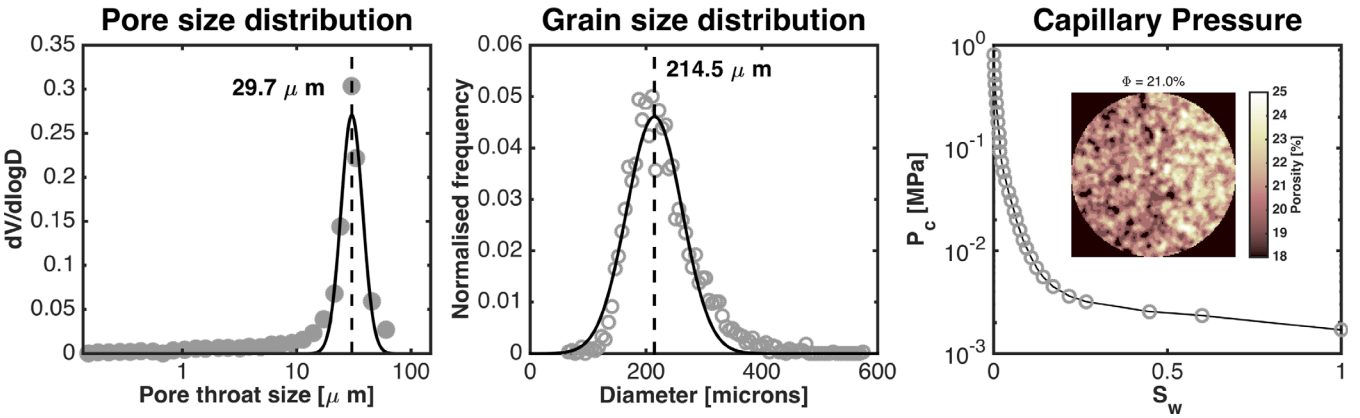

Figure 7. Pore size distribution, grain size distribution, and capillary pressure curve measured on microcores subsampled from experimental core.

the pressure drop across the core are also continuously recorded. An extra bypass line is used to equilibrate CO_2 and brine before injection into the core.

Fluid saturations are measured using a medical X-ray CT scanner (Universal Systems HD-350) using a voltage of 120 kV, current of 225 mA, and exposure time of 1 s. Scans of 1 mm thickness are taken at 5 mm intervals along the length of the core. The $x - y$ resolution of the images is 512 pixels or 234.4 μm.

Table 3. Measured Relative Permeability to CO_2 and Brine[a]

	f_{CO_2}	S_w	k_{r,CO_2}	$k_{r,w}$	ΔP (kPa)
Experiment 1	0.0929	0.6221	0.0014	0.1129	199.7
$scCO_2$-brine	0.2567	0.6131	0.0042	0.1017	181.7
38°C, 20.7 MPa	0.6065	0.5799	0.0150	0.0809	120.9
0 mol/kg NaCl	0.8739	0.5141	0.0405	0.0486	64.49
$q_T = 20$ mL/min	0.9700	0.4663	0.0844	0.0217	34.36
	0.9939	0.4035	0.1396	0.0072	21.30
	0.9984	0.3557	0.1901	0.0025	15.71
	0.9996	0.2880	0.2623	0.0009	11.40
Experiment 2	0.0640	0.7782	0.0015	0.3139	34.27
$scCO_2$-brine	0.2440	0.7185	0.0043	0.1885	46.09
91°C, 10.3 MPa	0.5918	0.6582	0.0137	0.1342	34.96
0 mol/kg NaCl	0.8662	0.6084	0.0456	0.1002	15.35
$q_T = 20$ mL/min	0.9562	0.5419	0.0864	0.0563	8.951
	0.9905	0.4544	0.1138	0.0155	7.039
	0.9982	0.3525	0.1806	0.0048	4.471
Experiment 3	0.1136	0.5901	0.0007	0.0821	365.2
$scCO_2$-brine	0.3036	0.5818	0.0022	0.0717	328.3
42°C, 13.5 MPa	0.5913	0.5754	0.0058	0.0565	244.8
3 mol/kg NaCl	0.8271	0.5459	0.0138	0.0410	142.8
$q_T = 20$ mL/min	0.9413	0.5109	0.0281	0.0249	79.91
	0.9822	0.4682	0.0536	0.0138	43.72
	0.9964	0.3879	0.1276	0.0065	18.63
	0.9994	0.3196	0.2118	0.0020	11.26
	0.9999	0.2748	0.2652	0.0006	8.995
Experiment 4	0.0013	0.8293	0.0000	0.4755	47.07
$scCO_2$-brine	0.0074	0.8107	0.0001	0.4604	48.31
65°C, 10.5 MPa	0.0312	0.8037	0.0005	0.3630	59.81
3 mol/kg NaCl	0.1076	0.7589	0.0012	0.2500	79.99
$q_T = 20$ mL/min	0.2956	0.7217	0.0034	0.2008	78.59
	0.5844	0.6746	0.0087	0.1550	60.10
	0.8229	0.6506	0.0237	0.1277	31.08
	0.9543	0.5569	0.0575	0.0690	14.85
	0.9899	0.4673	0.0839	0.0216	10.55
	0.9993	0.3649	0.1158	0.0022	7.716

[a]Experiments 1–4 performed at constant total flow, $q_T = 20$ mL/min.

Background X-ray CT scans of the core fully saturated with brine, CO_2 and CO_2-saturated brine at the experimental pressure, temperature, and salinity must be made prior to the beginning of the experiment. Porosity and saturation are calculated following *Akin and Kovscek* [2003].

After the background scans have been taken and baseline porosity measured, CO_2 and brine are circulated together outside the core in the bypass line for several hours to ensure both fluids are fully saturated with respect to one another, such that the displacements during the experiments are immiscible. Absolute permeability to CO_2-saturated brine is measured prior to beginning each drainage displacement (Figure 5). This setup procedure is employed before every core flood to ensure there is no change in pore

Table 4. Measured Relative Permeability to CO_2 and Brine[a]

	f_{CO_2}	S_w	k_{r,CO_2}	$k_{r,w}$	ΔP (kPa)
Experiment 5	0.1008	0.6441	0.0009	0.0989	232.9
$scCO_2$-brine	0.2198	0.6374	0.0020	0.0867	230.6
40°C, 10.7 MPa	0.4104	0.6252	0.0044	0.0793	190.6
0 mol/kg NaCl	0.6970	0.6032	0.0111	0.0598	129.7
$q_T = 20$ mL/min	0.8842	0.5673	0.0236	0.0383	77.34
	0.9501	0.5360	0.0413	0.0269	47.55
	0.9797	0.5059	0.0702	0.0181	28.80
	0.9921	0.4650	0.1058	0.0105	19.36
	0.9970	0.4248	0.1567	0.0057	13.14
	0.9996	0.3309	0.2421	0.0011	8.527
	0.9999	0.2870	0.2527	0.0003	8.173
Experiment 6	0.0112	0.8969	0.0006	0.7056	20.53
$scCO_2$-brine	0.0305	0.8762	0.0015	0.5805	24.47
85°C, 13.3 MPa	0.0763	0.8434	0.0030	0.4577	29.56
0 mol/kg NaCl	0.1731	0.7804	0.0055	0.3274	37.00
$q_T = 20$ mL/min	0.3419	0.7426	0.0101	0.2435	39.59
	0.5605	0.7055	0.0195	0.1914	33.64
	0.8850	0.6158	0.0603	0.0980	17.19
	0.9504	0.5576	0.0905	0.0589	12.31
	0.9852	0.4873	0.1311	0.0246	8.810
	0.9997	0.3349	0.2200	0.0007	5.327
Experiment 7	0.0466	0.6135	0.0002	0.0845	483.4
$scCO_2$-brine	0.1494	0.6163	0.0007	0.0764	477.4
41°C, 12.1 MPa	0.5215	0.5985	0.0032	0.0572	358.4
5 mol/kg NaCl	0.8293	0.5695	0.0095	0.0378	193.4
$q_T = 20$ mL/min	0.9229	0.5451	0.0177	0.0288	114.8
	0.9565	0.5283	0.0275	0.0243	76.74
	0.9760	0.5066	0.0397	0.0190	54.17
	0.9870	0.4804	0.0575	0.0148	37.85
	0.9931	0.4600	0.0852	0.0116	25.71
	0.9974	0.4256	0.1264	0.0065	17.40
	0.9991	0.3896	0.2003	0.0037	11.00
	0.9999	0.3129	0.2983	0.0009	7.394

[a]Experiments 5–7 performed at constant total flow, $q_T = 20$ mL/min.

structure between experiments and a full suite of background scans is taken at every experimental condition.

7. Experimental Conditions

Drainage core floods are performed in three sets (Table 1): first, using CO_2-brine and N_2-deionized water to investigate the impact of varying fluid properties such as interfacial tension (IFT) and viscosity contrast between fluid pairs, while keeping the total flow rate constant (Experiments 1–8); second, using N_2-deionized water with constant fluid properties, but varying the total flow rate of the displacement (Experiments 8–10); third, using N_2-deionized water with constant fluid properties and varying fractional flow (Experiments 11 and 12).

The conditions of Experiments 1–7 were chosen so as to represent the range of fluid properties that may be encountered for geological storage for supercritical CO_2 in a typical saline aquifer, while being able to isolate any change due to varying an individual fluid parameter (given in Table 2). Temperature and pressure conditions for the storage of supercritical CO_2 ($T_{crit} = 31$°C, $P_{crit} = 7.4$ MPa), at depths of ~0.8 to 3 km, range from 32 to 120°C and 7.5 to 30 MPa [*Nordbotten et al.*, 2005]. The change in fluid properties such as viscosity [*Fenghour et al.*, 1998; *Kestin et al.*, 1981] and IFT [*Li et al.*, 2012] with pressure, temperature, and salinity in the CO_2-brine system are well known. Interfacial tension varies from 25 to 50 mN/m, while viscosity ratio, $M = \mu_{CO_2}/\mu_{brine}$, ranges from 0.02 to 0.2, with most of the change coming from μ_{CO_2} [*Adams and Bachu*, 2002].

To isolate the independent impact of IFT and viscosity on relative permeability, CO_2-brine core floods were performed with NaCl brine molalities of 0, 3, and 5 mol/kg at pressure and temperature ranges of 10.3–20.7 MPa and 38–91°C. Conditions were selected so that pairs of experiments were performed at constant IFT and/or viscosity ratio but varying the CO_2 viscosity (Figure 6). All N_2-water core floods were performed at

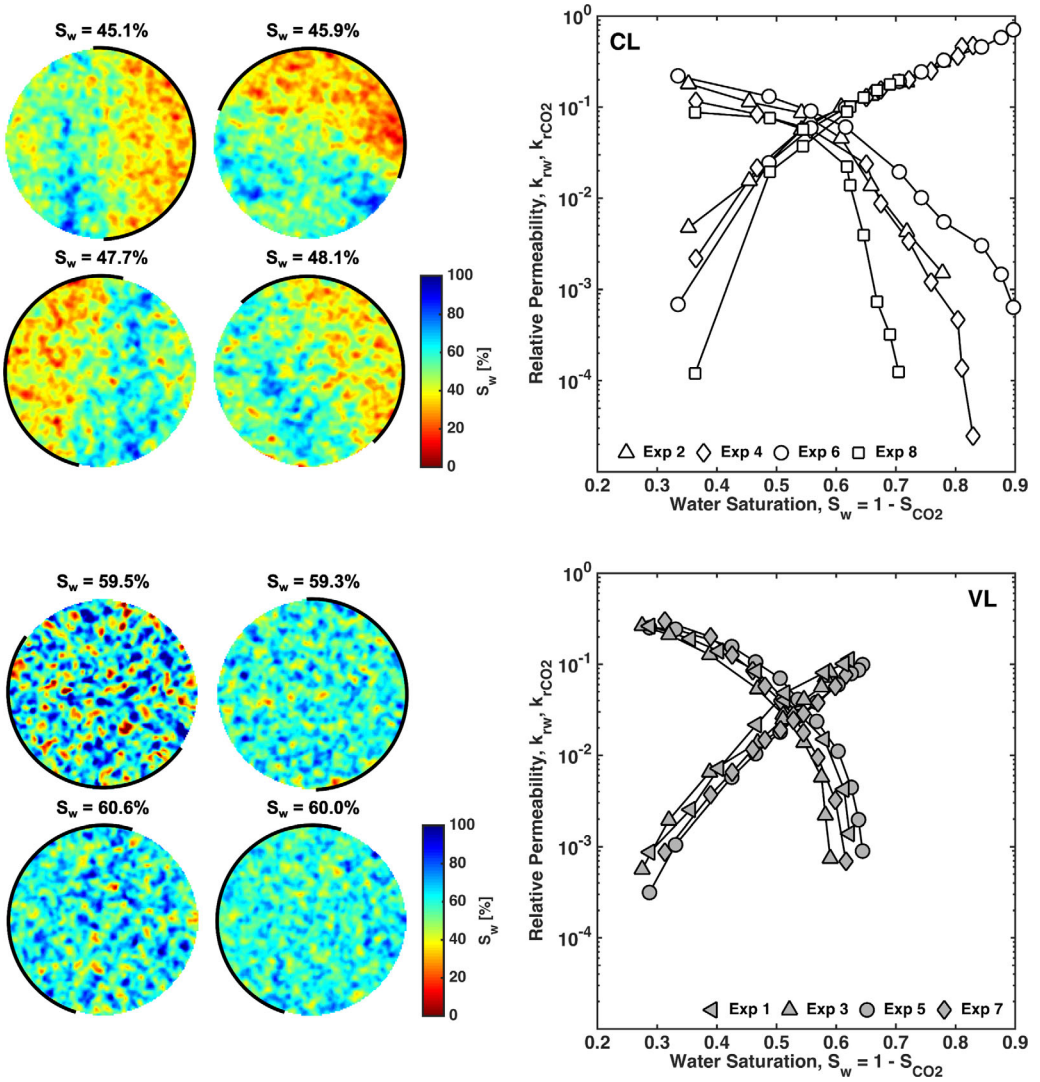

Figure 8. (left) Saturation maps for Experiments 1–7. Black line indicates high-permeability half of core. Top clockwise: Experiments 2, 4, 8, and 6. Bottom clockwise: Experiments 1, 3, 7, and 5. (right) Relative permeability curves for Experiments 1–8. (top) Capillary limited effective relative permeability. (bottom) Viscous limited intrinsic relative permeability.

15.5 MPa and 50°C with deionized water, while holding either total flow rate or the fractional flow of N_2 constant.

8. Rock Properties

Experiments are performed on a single Bentheimer sandstone core, 0.239 m in length (0.198 m for Experiments 1 and 9–12 after sampling for capillary pressure measurements) and 0.038 m diameter, composed of 95% quartz with minor feldspars (4%) and clays (1%) [*Andrew et al.*, 2014]. Absolute permeability to brine was measured in situ before each core flood at experimental conditions and was found to be 1.810 $\pm$ 0.033 D. The CT scanner-measured porosity was 22.2 $\pm$ 1.9%. The core has a unimodal pore and grain size distribution, with a modal pore diameter of 29.7 μm.

Grain and pore size distributions were measured on 4 $\times$ 10 mm subsamples taken from the experimental core, using a Versa XRM-500 micro-X-ray CT scanner (Figure 7, left and middle). Mercury intrusion capillary pressure (Figure 7, right) was measured on the same microcores using a Micromeritics Autopore IV 9500 Porosimeter and converted for CO_2.

Table 5. Measured Relative Permeability to N_2 and Deionized Water[a]

	f_{N_2}	S_w	k_{r,N_2}	$k_{r,w}$	ΔP (kPa)
Experiment 8	0.0155	0.7091	0.0001	0.1969	100.5
N_2-deionized water	0.0429	0.6958	0.0003	0.1780	108.1
50°C, 15.5 MPa	0.1069	0.6729	0.0007	0.1525	117.7
$q_T = 20$ mL/min	0.4334	0.6504	0.0039	0.1278	89.15
	0.7739	0.6226	0.0139	0.1013	44.89
	0.8615	0.6168	0.0222	0.0889	31.34
	0.9745	0.5436	0.0572	0.0373	13.78
	0.9898	0.4933	0.0761	0.0195	10.51
	0.9999	0.3794	0.0878	0.0001	9.204
Experiment 9	0.1429	0.6594	0.0008	0.1232	42.34
N_2-deionized water	0.4000	0.6309	0.0026	0.0979	37.27
50°C, 15.5 MPa	0.7143	0.6038	0.0069	0.0685	25.39
$q_T = 7$ mL/min	0.8857	0.5663	0.0131	0.0420	16.56
	0.9429	0.5413	0.0192	0.0290	12.00
	0.9929	0.4534	0.0364	0.0065	6.663
Experiment 10	0.0250	0.5606	0.0001	0.0700	493.8
N_2-deionized water	0.1000	0.5596	0.0003	0.0652	489.7
50°C, 15.5 MPa	0.3750	0.5418	0.0012	0.0511	434.1
$q_T = 40$ mL/min	0.6250	0.5310	0.0029	0.0427	311.3
	0.8250	0.5080	0.0063	0.0333	186.3
	0.9000	0.4872	0.0099	0.0273	129.9
	0.9500	0.4639	0.0151	0.0198	89.67
	0.9750	0.4470	0.0226	0.0144	61.46
	0.9875	0.4229	0.0320	0.0101	43.96
	0.9950	0.3866	0.0423	0.0053	33.57

[a]Experiments 8–10 performed at constant total flow rate.

The experimental core had a simple layered heterogeneity which can be seen in the CT-measured porosity (Figure 7, right inset) and is illustrated in Figure 1. The high-permeability layer has an average of 24.6 ± 0.09% porosity and a low-permeability layer with a 20.8 ± 0.03% porosity.

9. Results and Discussion

9.1. CO_2-Brine Core Floods at Constant Total Flow Rate

Eight drainage relative permeability curves were measured at a $q_T = 20$ mL/min, seven with CO_2 and brine, and one with N_2 and deionized water. Pairs of CO_2-brine experiments were performed at the same interfacial tension, but different fluid viscosities and densities. The measured relative permeability data are given in Tables 3 and 4.

Along-core saturation profiles were used to verify there were no significant end effects during the experiments and the calculated relative permeability was corrected where appropriate (Appendix A).The error in

Table 6. Measured Relative Permeability to N_2 and Deionized Water[a]

	q_T (mL/min)	S_w	k_{r,N_2}	$k_{r,w}$	ΔP (kPa)
Experiment 11	5	0.8083	0.0093	0.2319	10.44
N_2-deionized water	6	0.7970	0.0091	0.2275	11.32
50°C, 15.5 MPa	8	0.7812	0.0089	0.2212	15.53
$f_{N_2} = 0.5$	10	0.7411	0.0075	0.1866	23.00
	13.5	0.6689	0.0059	0.1358	41.10
	20	0.5643	0.0030	0.0752	128.7
	40	0.5730	0.0034	0.0838	231.2
	70	0.5679	0.0035	0.0873	388.2
Experiment 12	7	0.4534	0.0364	0.0065	6.663
N_2-deionized water	9	0.4426	0.0345	0.0062	9.051
50°C, 15.5 MPa	12	0.4439	0.0425	0.0076	9.794
$f_{N_2} = 0.993$	16	0.4434	0.0420	0.0075	13.20
	25	0.4399	0.0488	0.0084	18.53
	40	0.4352	0.0499	0.0089	27.79

[a]Experiments 11 and 12 performed at constant fractional flow of N_2.

saturation, given by the standard error in slice-averaged saturation for three sets of scans at each fractional flow, and the error in relative permeability, given by the standard error in the pressure drop measured during the scan time, are provided in Appendix B. For the majority of data points, the error is within the data symbol.

Two types of CO_2 distribution and relative permeability are observed. Under conditions with a low nonwetting phase viscosity (Experiments 2, 4, 6. and 8, $\mu_{CO_2} = 22.1–27.0$ μPa s), there is a discontinuity in saturation between the two halves of the core, with the higher nonwetting phase saturation in the high-porosity half, and the displacement appears to be heterogeneous (Figure 8, top left). The trend of higher S_{nw} in the high-permeability half of the core is apparent for all fractional flows for each low nonwetting phase viscosity experiment. The relative permeability to CO_2 shows significant spread at low CO_2 saturation (Figure 8, top right). The experiments are performed at different interfacial tensions (34–62 nM/m), so it appears this may be the fluid parameter with most influence on relative permeability.

Under conditions with a high nonwetting phase viscosity (Experiments 1, 3, 5, and 7, $\mu_{CO_2} = 52.7–81.8$ μPa s), the saturation distribution in the core is completely homogeneous and no influence of the pore space heterogeneity of the core is observed (Figure 8, bottom left). The relative permeability measured for these displacements all fall on the same set of curves (Figure 8, bottom right). These experiments are also performed at a similar range of interfacial tensions (29–41 mN/m), but in this case, the IFT seems to have no effect on relative permeability.

The major difference between the two sets, as has already been alluded to, is the nonwetting phase viscosity and the manifestation of this in the viscous pressure drive that can be achieved during the displacement (Figure 9). Displacements with a low nonwetting phase viscosity occur under capillary limited conditions ($N_c < 75$). Capillary-dominated cross flow occurs, where water imbibes into the low-permeability half of the core, resulting in a higher nonwetting phase saturation in the high-permeability side. The measured relative permeability is sensitive to the particular flow path the CO_2 takes, which is controlled by capillary forces. This can be thought of as an *effective* relative permeability which is a function of the particular flow conditions, and is affected by the nonwetting phase viscosity only in as far as this changes the capillary number of the displacement.

Displacements with a high nonwetting phase viscosity occur under viscous dominated conditions, so the nonwetting phase invades both sides of the core evenly, despite the heterogeneity in capillary pressure between the two. Under these conditions, a constant, *intrinsic* relative permeability curve is measured and no apparent dependence on other fluid properties (such as IFT) or through a change in wetting (due to changing brine salinity from 0 to 5 mol/kg NaCl) is observed. This viscous limit is the assumed condition for traditional steady state tests. However, the relative permeability curves produced may not be the most representative of the flow behavior at reservoir conditions (section 10).

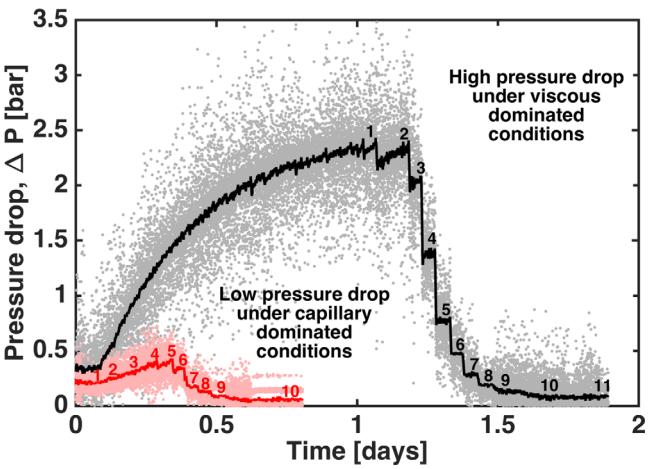

Figure 9. Typical viscous pressure drop, ΔP, during steady core floods under capillary (red) and viscous dominated (black) conditions. Experimental pressure drops for Experiments 5 and 6 with each fractional flow step numbered.

9.2. The Effect of Interfacial Tension on CO_2-Brine Relative Permeability

We can compare pairs of experiments performed at the same IFT but with different nonwetting phase viscosity (Figure 10) and see that IFT is not the cause of changes in relative permeability, but rather the switch from capillary cross flow dominated conditions at low CO_2 viscosity to viscous dominated at high CO_2 viscosity.

This suggests that observations of a dependence of CO_2-brine relative permeability from other authors are in fact a manifestation of this same effect. In particular, *Bachu and Bennion* [2008] observe a decrease in relative

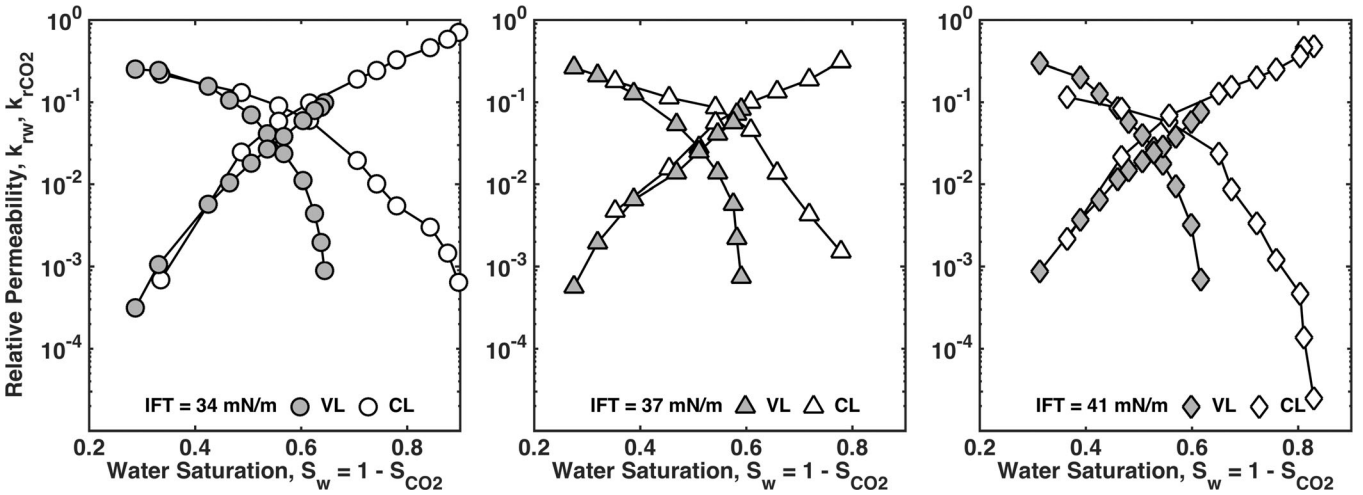

Figure 10. Relative permeability plotted for constant interfacial tension, but varying CO_2 viscosity. Grey symbols indicate characteristic viscous-dominated displacements and white symbols indicate capillary-dominated displacements.

permeability to brine and CO_2 concurrent with an increase in IFT from 19.8 to 56.2 mN/m (Figure 11). However, this increase in interfacial tension is achieved simply by increasing the experimental pressure from 1.4 to 20 MPa, resulting in a fourfold increase in CO_2 viscosity from 16 to 75 μPa s. It is likely that this increase is enough to change the force balance for the displacement, and hence change the influence of capillary heterogeneity in the core. We discuss identifying the threshold at which core a core flood will go from being capillary to viscous dominated fully in section 10.

9.3. Core Floods Varying Total Flow Rate Using N_2 and Deionized Water

In order to confirm that the observed changes in relative permeability in Experiments 1–8 are due to the viscous-capillary force balance and not due to changes in fluid properties, we perform further steady state drainage experiments between N_2 and deionized water. Experiments 8–12 are performed at constant pressure temperature and salinity conditions. To rule out any impact of using CO_2 as the nonwetting phase, full drainage relative permeability curves are measured for different total flow rates (Experiments 8–10), where increasing the total flow rate will increase the viscous pressure drop in the same way that increasing CO_2 viscosity did for the CO_2-brine core floods. The transition from capillary-dominated effective relative permeability curves to viscous-dominated intrinsic relative permeability curves is further investigated by measuring point values of relative permeability at a constant fractional flow, while varying the total flow rate (Experiments 11 and 12). Tabulated results are given in Tables 5 and 6.

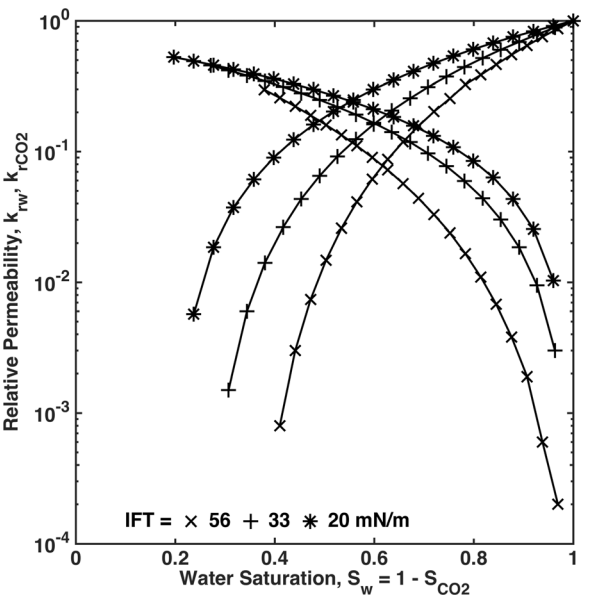

Figure 11. Unsteady state relative permeability data replotted from *Bachu and Bennion* [2008].

We find that, just as for the CO_2-brine system, increasing the viscous pressure drop by increasing the total flow rate of the displacement results in a change from capillary cross flow (which creates a higher N_2 saturation in the high-permeability half of the core) toward a viscous-dominated displacement, where N_2 invades both layers equally (Figure 12). Concurrent with this, the relative permeability curves shift toward lower water saturation and the nonwetting phase relative permeability decreases at a given saturation

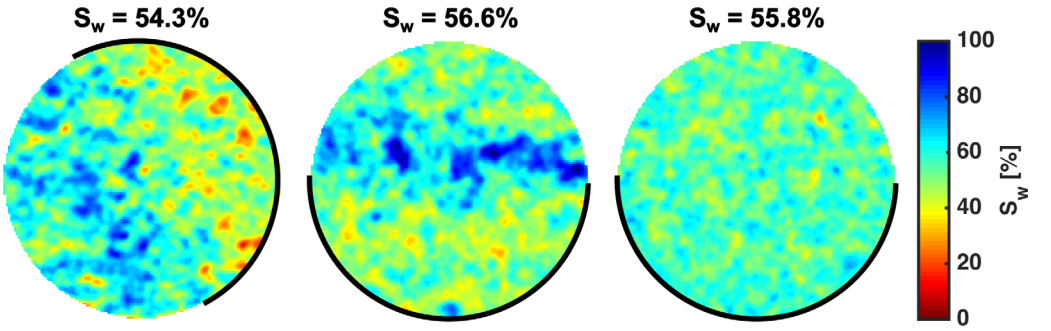

Figure 12. Saturation maps for N_2-water core floods performed at constant total flow rate. From left to right, Experiments 8–10. Black line indicates high-permeability half of core.

(Figure 13). *Krause and Benson* [2015] model changes in relative permeability toward the viscous limit using an accurate characterization of subcore-scale heterogeneity and find that the heterogeneity controls the manner in which relative permeability changes. This suggests that the decrease in nonwetting phase relative permeability toward the viscous limit observed in Figures 10 and 13 is a result of the specific heterogeneity present in the core sample, rather than a general trend.

10. Scaling Heterogeneity in CO_2-Brine Core Floods

The capillary number, N_c (equation (2)), defined by *Virnovsky et al*. [2004] and described in section 3 can be used to characterize the viscous-capillary force balance during the drainage displacements presented. We can use the measured core dimensions L and H and the experimental viscous pressure drop ΔP directly, but must derive $|\Delta P_c(f_w)|$ from the measured capillary pressure curve for the Bentheimer core and the observed contrast in saturation between high-permeability and low-permeability halves of the core during capillary-dominated displacements (e.g., Figure 8, top left).

Egermann and Lenormand [2005] found that capillary pressure heterogeneity within a rock core is better estimated by saturation profiles rather than pressure profiles. Under steady state, capillary-dominated conditions, we can assume that the observed contrast in saturation between the two halves of the Bentheimer core occurs due to a contrast in capillary pressure (Figure 2, red line). The measured capillary pressure curve is assigned to the high-permeability layer and we assume that the capillary pressure curve for the lower-permeability layer takes the same form, but is simply shifted to lower values of CO_2 saturation. The shift is estimated at each steady state fractional flow for Experiments 2, 4, and 6 using the contrast in saturation observed in the CT images (Figure 8, top left). Thus, by moving each point on the capillary pressure curve to the lower saturation observed in the images, a new capillary pressure curve for the low-permeability layer is created (Figure 14). The vertical difference between capillary pressure curves at the steady state saturation of a specified fractional flow gives the contrast in capillary pressure, $|\Delta P_c(f_w)|$. For the core used in this experimental study, the average contrast in capillary pressure is approximately 500 Pa. This contrast is too low to be identified by tracer testing, and as such would be characterized as a homogeneous core. However, it is clear from the data presented in this work that the CO_2-brine system is extremely sensitive even to minor capillary pressure heterogeneity.

Capillary numbers for this data set range from 10^{-1} to 10^{3} (Figure 15). We define core floods displaying heterogeneous distributions of CO_2, that are clearly influenced by the high-permeability and low-permeability sides of the core, as capillary dominated and core floods with homogeneous distributions of CO_2 as viscous dominated. By this definition, the transition occurs at around 50–100, but this is saturation and fractional flow dependent. The transition to the viscous limit occurs at capillary numbers as low as 0.1 for very high nonwetting phase fractional flow ($>$0.85), however, this is still in the transition range predicted by *Virnovsky et al*. [2004]. In order to perform a full steady state drainage experiment under viscous-dominated conditions and measure the intrinsic relative permeability, the starting fractional flow must be at capillary numbers greater than the upper bound for the transition.

The exact value of N_c at which the transition occurs is dependent on the particular heterogeneity of the core sample. Given the extraordinarily low characteristic capillary pressure contrast of the core sample used

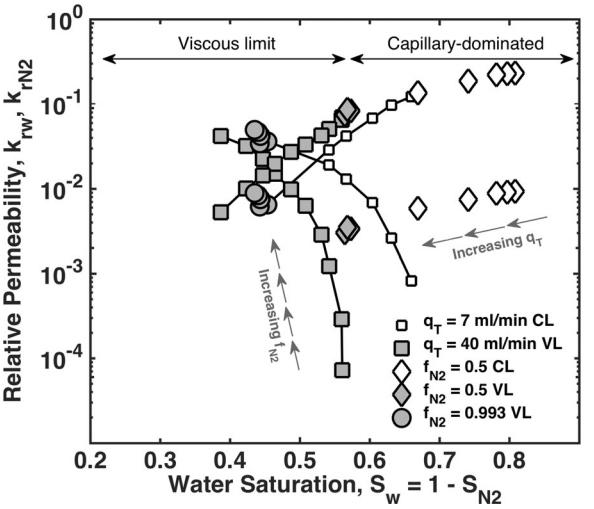

Figure 13. Effective and characteristic drainage relative permeability curves measured using N_2 and deionized water at constant pressure and temperature, but varying total flow rate and hence viscous pressure drive.

in this study, we expect $N_c \approx 75$ to form a minimum bound at which steady state *intrinsic* relative permeability should be measured in sandstones.

Capillary number is calculated for all CO_2-brine steady state drainage relative permeability data sets reported in the literature, for which fractional flow data are reported [*Akbarabadi and Piri*, 2013; *Bachu and Bennion*, 2008; *Bennion and Bachu*, 2008, 2006b, 2006a, 2005; *Kogure et al.*, 2013; *Krause et al.*, 2013; *Krevor et al.*, 2012; *Manceau et al.*, 2015; *Perrin and Benson*, 2010; *Pini and Benson*, 2013; *Ruprecht et al.*, 2014; *Zhang et al.*, 2013]. If ΔP is not reported, this is calculated from the data provided using the multiphase extension to Darcy's law (equation (4)). An average $|\Delta P_c(f_w)|$ is calculated from reported capillary pressure curves, or the capillary entry pressure is used. For experiments performed on Berea sandstone, a $\Delta P_c = 5000$ Pa is used [*Pini et al.*, 2012]. The majority of data sets fall below $N_c = 75$ (Figures 3 and 16) and all fall below $N_c = 10^2$. We suggest that for the majority of core samples, the transition to the viscous limit will occur at $N_c > 10^2$ and that almost all reported CO_2-brine relative permeability curves are measured in the capillary-dominated regime. This can be confirmed by CT-measured saturation where available. It is therefore unsurprising that many authors find relative permeability to be influenced in some way by the reservoir conditions of the experiment—in the capillary-dominated regime, relative permeability will be sensitive to flow rate and reservoir conditions.

11. Representing Reservoir Flow Using Effective and Intrinsic Relative Permeability

To provide a comparison with field-scale flow behavior, capillary numbers are estimated for CO_2 flow and oil recovery under gravity, water flood of an oil reservoir, and injection of CO_2 near wellbore and in the far field in a high-permeability, clean sandstone reservoir, using $H = 20$ m, $L = 500$ m far field and 10 m near wellbore, $\Delta P_c = 5$ kPa (Figure 17). Typical pressure drops of 2 and 8 kPa/m for gas and oil, respectively, for gravity-driven recovery, give $N_c \approx 0.3$–1.3 [*Dake*, 1983]; 6–12 kPa/m for water flood recovery of a typical oil field gives $N_c \approx 25$–50 and near wellbore, where viscous pressure drops may be 5 times greater, $N_c \approx 100$–250 [*Sorbie et al.*, 1982; *Taber*, 1969]; for CO_2 injection into an open aquifer such as at the Sleipner site, pressure drops are of order 0.002–0.2 kPa/m in the far field, and ≈1 kPa near wellbore, giving $N_c \approx 0.01$–1.2 and $N_c \approx 4$, respectively [*Chadwick et al.*, 2012]; in a more compartmentalized reservoir such as the Gorgon field, pressure drops may be in excess of 10 kPa/m, giving $N_c \approx 40$ [*Flett et al.*, 2009].

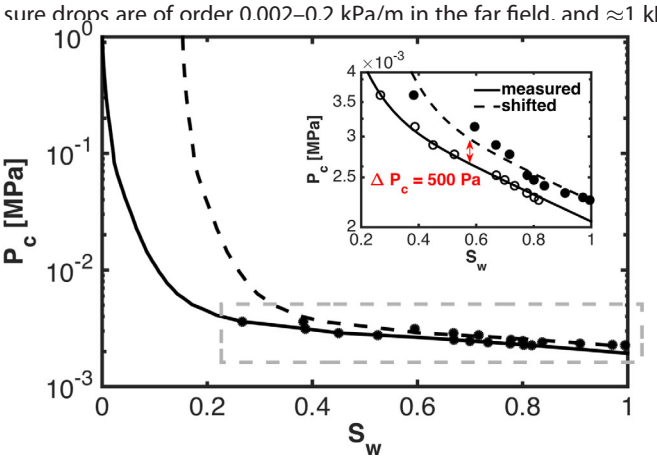

Figure 14. Measured and shifted capillary pressure curves for each side of the Bentheimer core.

For both CO_2 and hydrocarbon fluid systems, far field reservoir flow behavior may occur under capillary limited conditions (Figure 17). For CO_2 storage sites in particular, there is a wide range of capillary numbers that may be representative of the flow behavior in a single reservoir. Therefore, it is essential to characterize the relative permeability

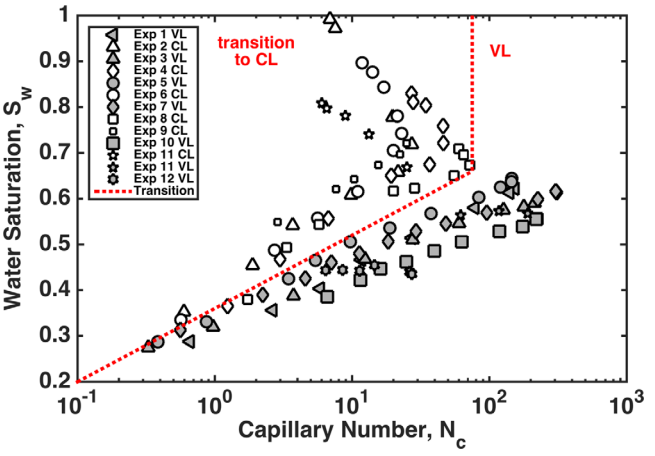

Figure 15. Water saturation, S_w, versus Capillary number, N_c, for CO_2-brine and N_2-deionized water core floods. The transition between capillary and viscous limited (CL to VL) is obtained empirically, using the observed steady state fluid distributions in the core. This occurs at $N_c \approx 75$ for $S_w < 0.65$.

and flow behavior under the appropriate conditions.

Traditionally, relative permeability curves are measured in the viscous limit, and these intrinsic relative permeability curves are then used to predict flow at the reservoir scale. Core-scale relative permeability curves usually undergo an upscaling procedure before being used as the input into reservoir models [*Kyte and Berry*, 1975; *Barker and Dupouy*, 1999]. If the geological system is particularly heterogeneous, this involves a laborious process of characterizing individual strata from separate core samples, then combining multiple laboratory-measured relative permeability curves into a single relative permeability curve [*Corbett et al*., 1992; *Ringrose et al*., 1993].

The recent work of *Krause and Benson* [2015] gives a detailed procedure for obtaining intrinsic relative permeability, i.e., in the viscous limit. But in order to properly represent the flow behavior on the reservoir, the effective relative permeability, or capillary limited, contains the most useful information. This has already been identified as a key shortcoming of traditional core analysis techniques for the hydrocarbon-brine system by *Ringrose et al*. [1993]. *Rabinovich et al*. [2015] recently developed an upscaling procedure for CO_2 injection into heterogeneous reservoirs whereby capillary pressure curves in a fine resolution grid are upscaled in the capillary limit. They find that the relative permeability calculated from the upscaled capillary pressure curves are flow rate dependent and suggest deriving relative permeability curves at each order of magnitude change in flow rate expected in the reservoir.

We suggest that in order to properly characterize the flow behavior in a reservoir, measurements can and should be made on heterogeneous samples. The number of samples required will depend on the specific geology of the reservoir—the number of rock types present, how they are arranged, and the structural variability present within a single rock type. Best practice for special core analysis in industry often requires the most homogeneous samples to be selected for core floods. However, in most reservoirs, the majority of core samples will display some heterogeneity. This suggests that measuring relative permeability

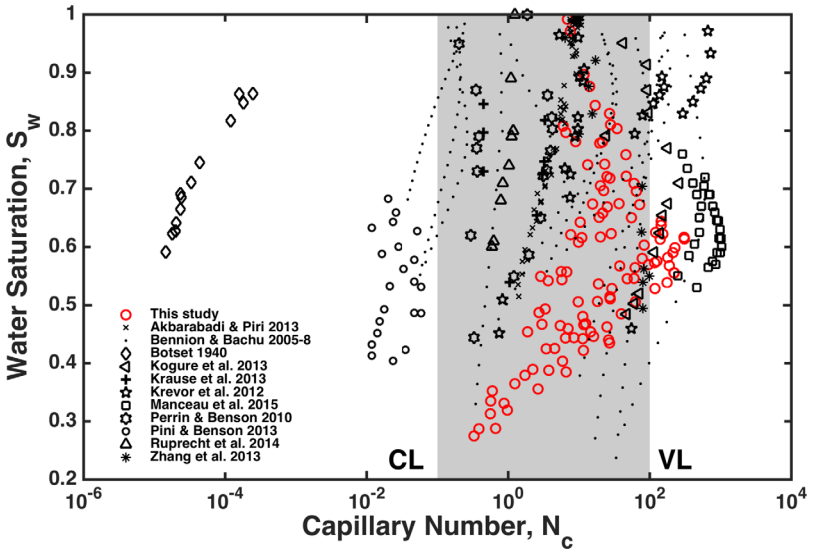

Figure 16. Compilation of capillary number-saturation data for drainage CO_2-brine relative permeability core floods from *Akbarabadi and Piri* [2013], *Bachu and Bennion* [2008], *Bennion and Bachu* [2008, 2006b, 2006a, 2005], *Kogure et al*. [2013], *Krause et al*. [2013], *Krevor et al*. [2012], *Manceau et al*. [2015], *Perrin and Benson* [2010], *Pini and Benson* [2013], *Ruprecht et al*. [2014], and *Zhang et al*. [2013]. Grey shading shows transition from CL to VL [*Virnovsky et al*., 2004].

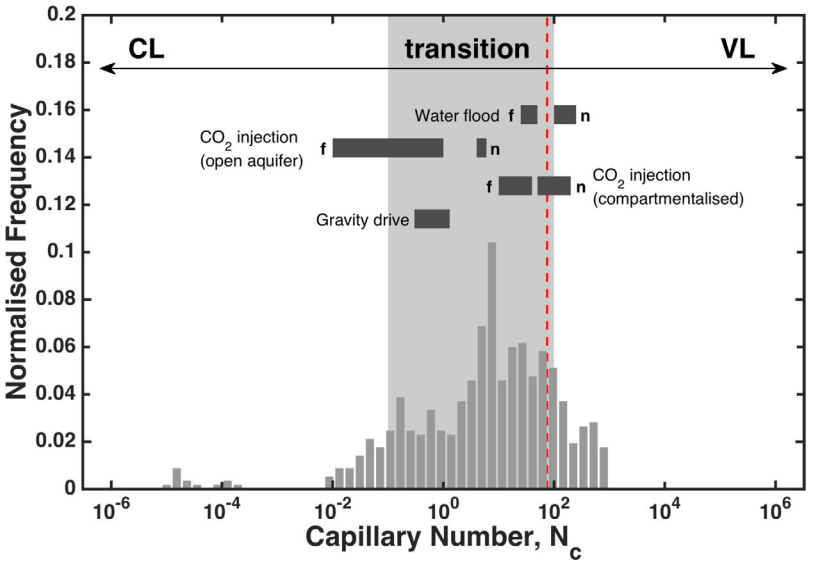

Figure 17. Histogram of capillary number under which steady state drainage relative permeability has been measured [*Akbarabadi and Piri*, 2013; *Bennion and Bachu*, 2005, 2006a, 2006b; *Bachu and Bennion*, 2008; *Bennion and Bachu*, 2008; *Perrin and Benson*, 2010; *Krevor et al.*, 2012; *Kogure et al.*, 2013; *Krause et al.*, 2013; *Pini and Benson*, 2013; *Zhang et al.*, 2013; *Ruprecht et al.*, 2014; *Manceau et al.*, 2015]. Transition from capillary limit (CL) to viscous limit (VL) is expected in the range $10^{-1} < N_c < 10^3$ (grey bar) [*Virnovsky et al.*, 2004] and occurs at $N_c \approx 75$ (red dashed line) for the data set in this study. Estimates of N_c for CO_2 injection and water flood of oil and gas fields near the wellbore (n) and in the far field (f) are explained in the text.

on the heterogeneous samples will provide as better description of the flow behavior in the reservoir as a whole. We emphasize that it is not necessary to make measurements on homogeneous cores representative of each stratal element, and that where appropriate, cores with the characteristic heterogeneity of the reservoir can be used. Relative permeability should be measured over the range of capillary numbers expected from near wellbore to the far field. Typically, this will mean only two or three measurements are required to represent flow behavior over 1 or 2 order of magnitude in capillary number. Normal upscaling techniques can be employed to use the measured relative permeability in reservoir models.

12. Conclusions

We have performed drainage core floods using CO_2-brine and N_2-deionized water and measured steady state relative permeability on a single sandstone rock core in order to fully characterize the flow behavior of the CO_2-brine system in simple heterogeneous rocks. Our conclusions are as follows:

1. CO_2-brine relative permeability is invariant over reservoir conditions of 10.3–20.7 MPa, 38–91°C, and 0–5 mol/kg NaCl brine so long as relative permeability is measured in the viscous limit.
2. Relative permeability is affected by capillary pressure heterogeneity when measured under capillary limited conditions. The transition from capillary limited to viscous limited flow and the impact on the effective flow functions is observed in both CO_2-brine systems and N_2-brine systems by varying either the fluid viscosity or fluid flow rates. Thus, the scaling proposed by a number of authors for heterogeneous systems [*Yokoyama and Lake*, 1981; *Zhou et al.*, 1997; *Jonoud and Jackson*, 2008; *Virnovsky et al.*, 2004] in which capillary pressure contrast and the experimental viscous pressure drop are compared, is demonstrated to be correct, albeit not predictive or universal, as we see the same impact on the flow behavior due to increasing the nonwetting phase viscosity or the fluid flow velocity. Capillary limited measurements of relative permeability are sensitive to flow rate and nonwetting phase viscosity in that these parameters control the viscous pressure drop achievable during a core flood and hence the capillary number of the displacement.
3. We use the N_c suggested by *Virnovsky et al.* [2004] to show that the vast number of reported observations of relative permeability for CO_2-brine systems were made in a system far from the viscous limit for the derivation of relative permeability. Hence any reported variance in relative permeability with

reservoir conditions is the result of making observations in a capillary limited system. This demonstrates that the reported heterogeneity in fluid distribution within the core [*Perrin and Benson*, 2010; *Zhang et al*., 2014] is thus the expected outcome of making observations at these conditions and that derived measures of relative permeability were also strongly controlled by the level of capillary heterogeneity in the system [*Virnovsky et al*., 2004].

4. The particular sensitivity of the CO_2-brine system to capillary heterogeneity is due to the low value and wide range of CO_2 viscosity over typical reservoir pressures and temperatures. This sensitivity has been used previously as the basis for suggesting that the wetting state of the CO_2-brine system is distinct from other water-wet systems and also uniquely sensitive to changes in interfacial tension. However, it is rather that the balance of viscous and capillary forces in the system can be changed dramatically with relatively small changes in experimental conditions.
5. Effective relative permeability curves may be produced directly from core-scale measurements by selecting cores with the characteristic capillary heterogeneity of a target reservoir and performing end-member steady state measurements to produce the intrinsic and minimum flow rate effective relative permeability curves at capillary numbers relevant to the reservoir.

Appendix A: Steady State Saturation Profiles

Steady state saturation profiles are used to check for end effects for each relative permeability measurement made (Figures 18–29). In general, saturation profiles show little (<10%) or no gradient in saturation

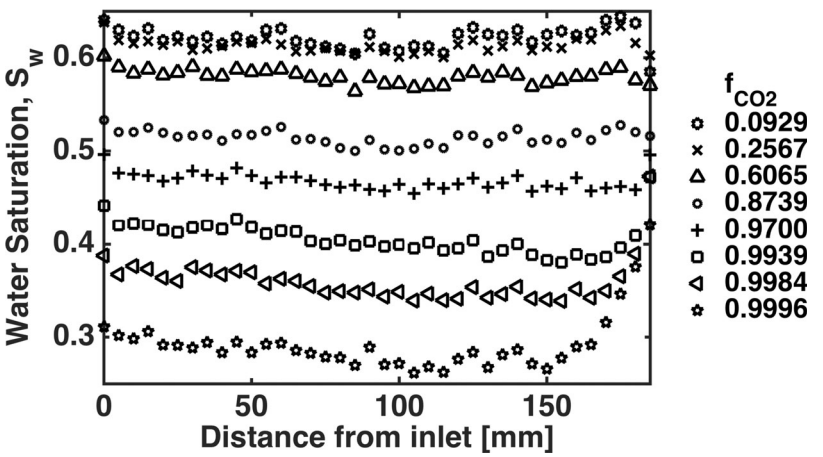

Figure 18. Experiment 1.

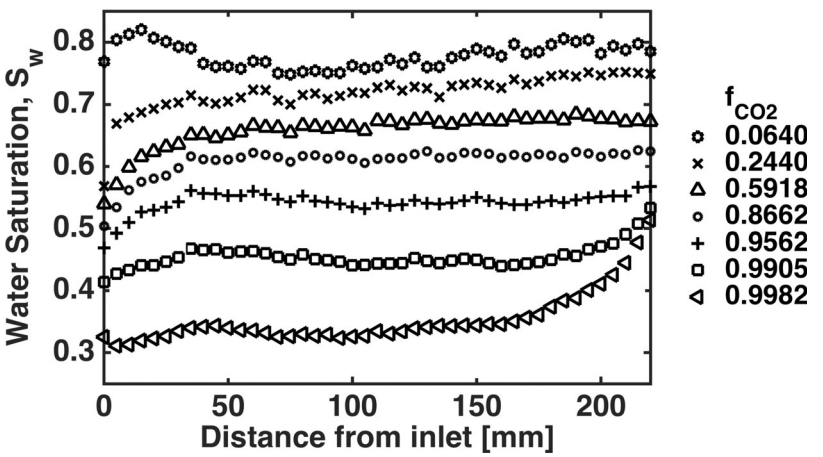

Figure 19. Experiment 2.

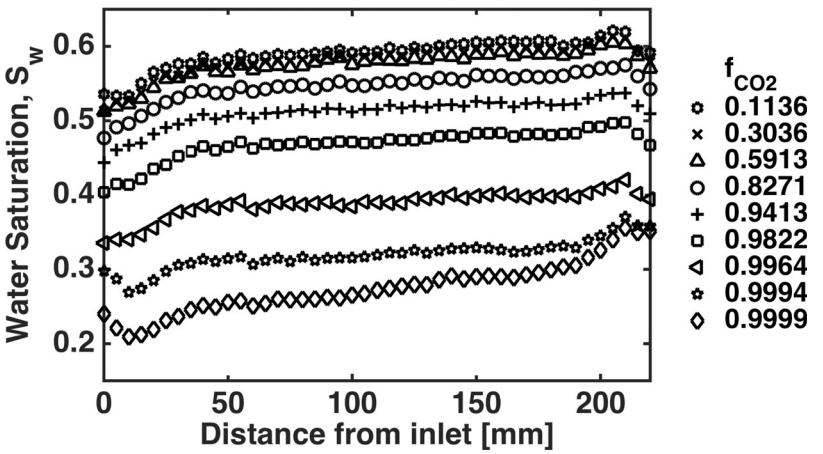

Figure 20. Experiment 3.

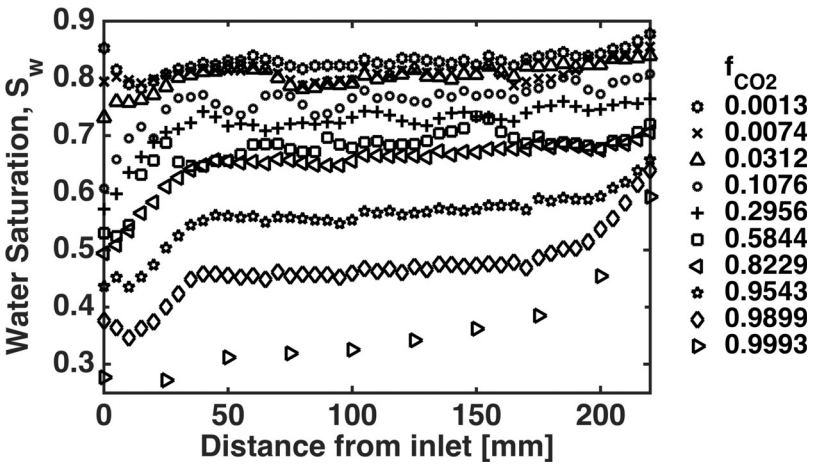

Figure 21. Experiment 4.

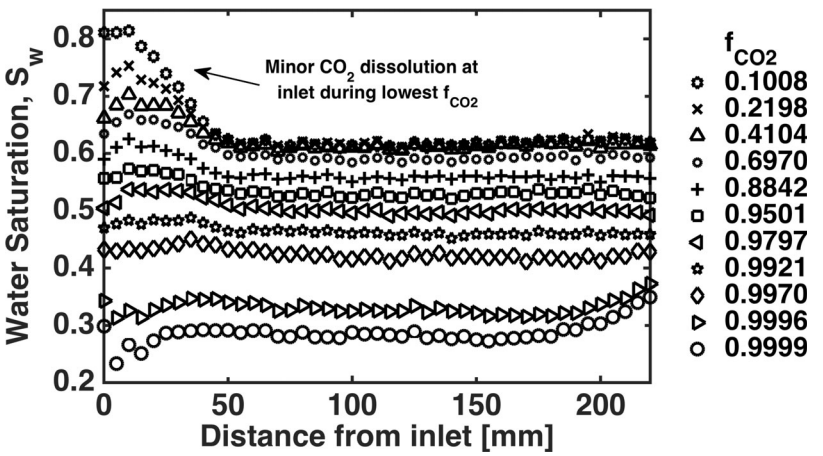

Figure 22. Experiment 5.

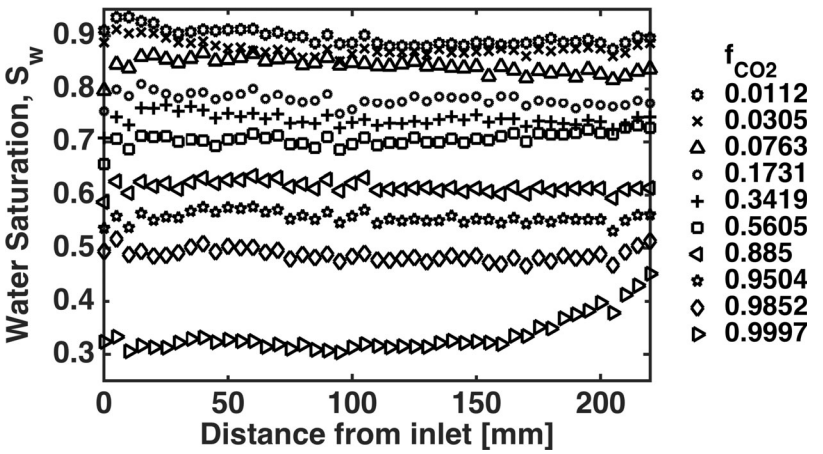

Figure 23. Experiment 6.

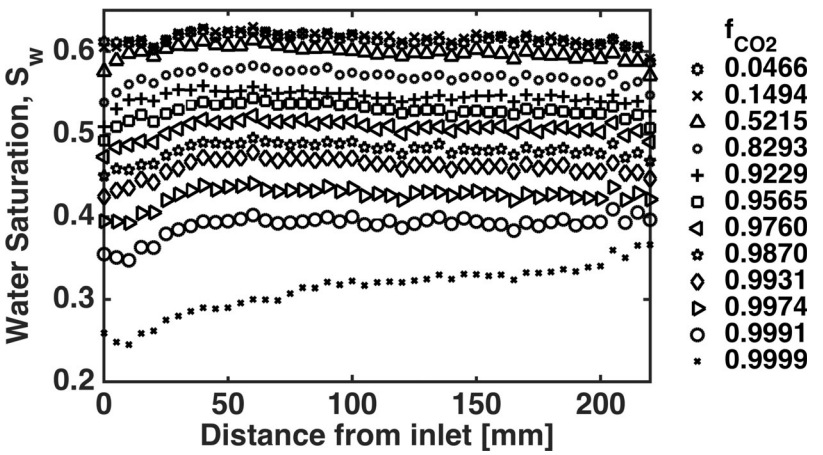

Figure 24. Experiment 7.

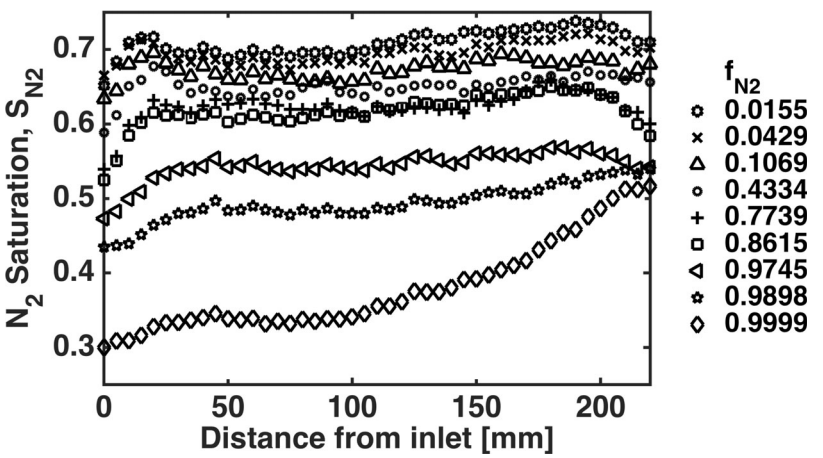

Figure 25. Experiment 8.

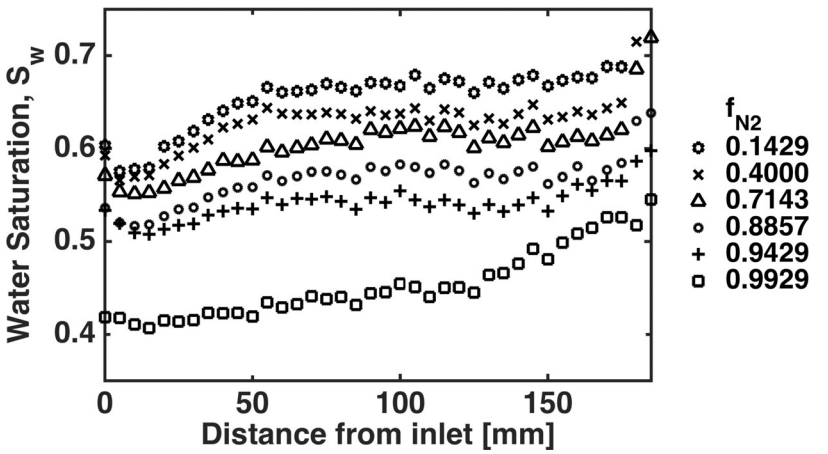

Figure 26. Experiment 9.

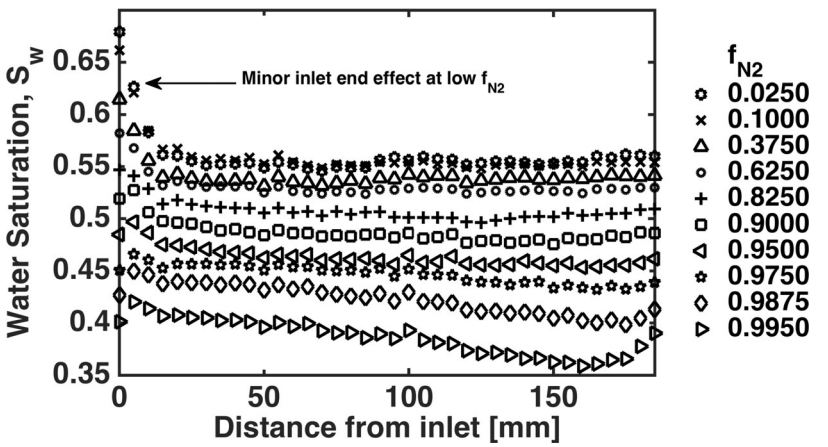

Figure 27. Experiment 10.

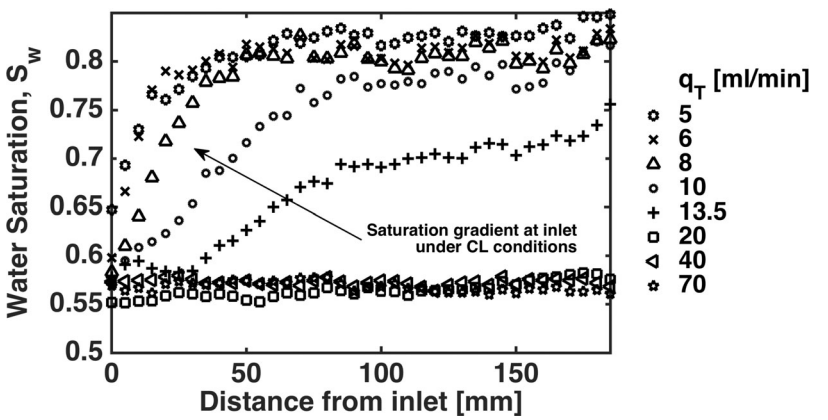

Figure 28. Experiment 11.

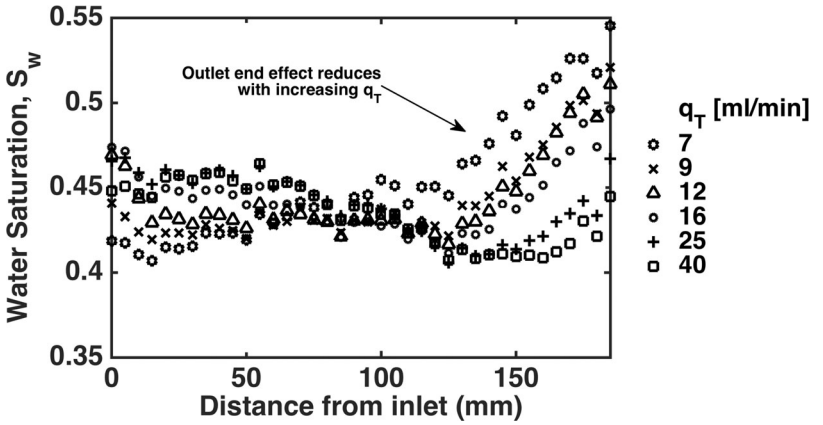

Figure 29. Experiment 12.

and show a consistent shape for the duration of each experiment. Outlet end effects are only observed for fractional flows >0.999. In each case, the core-averaged saturation has been corrected by using the saturation observed in the portion of the core without end effects. Where there are end effects we use Sendra, a two-phase simulator designed to verify core flood experiments, to predict what the pressure drop would be with no saturation gradient. Slice average saturation profiles, the measured pressure drop, and calculated relative permeabilities for all of the fractional flow steps unaffected by end effects are used as input data. The pressure drop for the fractional flow with end effects is estimated for the corrected core-averaged saturation. The error in the pressure drop and hence in the calculated relative permeability is less than the standard error (Appendix B) or within the data symbol in all cases (Figure 8). *Gupta and Maloney* [2015] describe an intercept method for correcting relative permeability measurements for end effects when fractional flows are performed at multiple flow rates. Relative permeability calculations for Experiments 11 and 12 are corrected for end effects using this method, but in both cases, the change in relative permeability is within the data symbol in Figure 13.

Appendix B: Error in Calculated Relative Permeability and Measured Fluid Saturations

Tabulated errors are provided for core-averaged fluid saturation and relative permeability for Experiments 1–12 (Tables B1–B4). For saturation, this is the standard error calculated from three sets of scans at each fractional flow. The error in relative permeability is given by the standard error of the pressure drop measured while taking three scans of the core at a single steady state fractional flow.

Table B1. Error in Relative Permeability and Saturation Measurements, Experiments 1–7

	S_w	k_{r,CO_2}	$k_{r,w}$
Experiment 1	0.0065	0.0000	0.0008
$scCO_2$-brine	0.0064	0.0001	0.0016
38°C, 20.7 MPa	0.0064	0.0003	0.0018
0 mol/kg NaCl	0.0066	0.0024	0.0029
$q_T = 20$ mL/min	0.0065	0.0081	0.0021
	0.0067	0.0114	0.0006
	0.0072	0.0285	0.0004
	0.0080	0.0078	0.0000
Experiment 2	0.0026	0.0000	0.0043
$scCO_2$-brine	0.0034	0.0001	0.0023
91°C, 10.3 MPa	0.0031	0.0001	0.0014
0 mol/kg NaCl	0.0027	0.0012	0.0027
$q_T = 20$ mL/min	0.0023	0.0063	0.0041
	0.0027	0.0062	0.0008
	0.0047	0.0253	0.0007
Experiment 3	0.0039	0.0000	0.0003
$scCO_2$-brine	0.0040	0.0000	0.0002
42°C, 13.5 MPa	0.0039	0.0000	0.0002
3 mol/kg NaCl	0.0040	0.0001	0.0004
$q_T = 20$ mL/min	0.0040	0.0002	0.0002
	0.0042	0.0012	0.0003
	0.0043	0.0048	0.0002
	0.0048	0.0056	0.0001
	0.0057	0.0115	0.0000
Experiment 4	0.0024	0.0000	0.0092
$scCO_2$-brine	0.0032	0.0000	0.0272
65°C, 10.5 MPa	0.0043	0.0000	0.0063
3 mol/kg NaCl	0.0046	0.0000	0.0036
$q_T = 20$ mL/min	0.0039	0.0000	0.0021
	0.0070	0.0004	0.0080
	0.0053	0.0006	0.0033
	0.0054	0.0021	0.0025
	0.0053	0.0020	0.0005
	0.0303	0.0092	0.0002

Table B2. Error in Relative Permeability and Saturation Measurements, Experiments 1–7

	S_w	k_{r,CO_2}	$k_{r,w}$
Experiment 5	0.0065	0.0000	0.0004
$scCO_2$-brine	0.0051	0.0000	0.0004
40°C, 10.7 MPa	0.0043	0.0000	0.0009
0 mol/kg NaCl	0.0042	0.0002	0.0009
$q_T = 20$ mL/min	0.0041	0.0004	0.0006
	0.0040	0.0007	0.0005
	0.0039	0.0016	0.0004
	0.0039	0.0032	0.0003
	0.0040	0.0130	0.0005
	0.0043	0.0305	0.0001
	0.0046	0.0235	0.0000
Experiment 6	0.0023	0.0000	0.0159
$scCO_2$-brine	0.0025	0.0000	0.0117
85°C, 13.3 MPa	0.0021	0.0001	0.0096
0 mol/kg NaCl	0.0024	0.0001	0.0052
$q_T = 20$ mL/min	0.0024	0.0002	0.0044
	0.0029	0.0004	0.0037
	0.0022	0.0013	0.0020
	0.0023	0.0041	0.0027
	0.0026	0.0070	0.0013
	0.0045	0.0043	0.0000
Experiment 7	0.0027	0.0000	0.0004
$scCO_2$-brine	0.0027	0.0000	0.0004
41°C, 12.1 MPa	0.0027	0.0000	0.0003
5 mol/kg NaCl	0.0028	0.0001	0.0005
$q_T = 20$ mL/min	0.0028	0.0004	0.0007
	0.0028	0.0010	0.0009
	0.0029	0.0006	0.0003
	0.0029	0.0011	0.0003
	0.0029	0.0021	0.0003
	0.0030	0.0035	0.0002
	0.0032	0.0092	0.0002
	0.0042	0.0381	0.0001

Table B3. Error in Relative Permeability and Saturation Measurements, Experiments 8–10

	S_w	k_{r,N_2}	$k_{r,w}$
Experiment 8	0.0029	0.0000	0.0021
N_2-deionized water	0.0028	0.0000	0.0019
50°C, 15.5 MPa	0.0026	0.0000	0.0015
$q_T = 20$ mL/min	0.0025	0.0001	0.0019
	0.0030	0.0002	0.0017
	0.0029	0.0004	0.0016
	0.0027	0.0011	0.0007
	0.0030	0.0015	0.0004
	0.0052	0.0020	0.0000
Experiment 9	0.0042	0.0000	0.0015
N_2-deionized water	0.0036	0.0000	0.0015
50°C, 15.5 MPa	0.0034	0.0002	0.0016
$q_T = 7$ mL/min	0.0028	0.0004	0.0012
	0.0023	0.0009	0.0014
	0.0040	0.0042	0.0008
Experiment 10	0.0025	0.0000	0.0005
N_2-deionized water	0.0023	0.0000	0.0005
50°C, 15.5 MPa	0.0028	0.0000	0.0005
$q_T = 40$ mL/min	0.0016	0.0000	0.0005
	0.0016	0.0001	0.0005
	0.0016	0.0002	0.0007
	0.0016	0.0005	0.0007
	0.0015	0.0011	0.0007
	0.0018	0.0011	0.0003
	0.0020	0.0026	0.0003

Table B4. Error in Relative Permeability and Saturation Measurements, Experiments 11 and 12

	S_w	k_{r,N_2}	$k_{r,w}$
Experiment 11	0.0048	0.0008	0.0195
N_2-deionized water	0.0046	0.0010	0.0242
50°C, 15.5 MPa	0.0060	0.0009	0.0213
$f_{N_2} = 0.5$	0.0072	0.0007	0.0165
	0.0059	0.0005	0.0121
	0.0024	0.0003	0.0076
	0.0020	0.0004	0.0092
	0.0019	0.0004	0.0101
Experiment 12	0.0040	0.0042	0.0008
N_2-deionized water	0.0030	0.0033	0.0006
50°C, 15.5 MPa	0.0028	0.0022	0.0004
$f_{N_2} = 0.993$	0.0024	0.0031	0.0006
	0.0022	0.0023	0.0004
	0.0025	0.0054	0.0010

Acknowledgments
This work was performed as part of the PhD thesis of Catriona Reynolds, funded by a departmental scholarship from the Department of Earth Science and Engineering, Imperial College London, provided by EPSRC. Experiments were performed in the Qatar Carbonates and Carbon Storage Research Centre at Imperial College London, funded jointly by Shell, Qatar Petroleum, and the Qatar Science and Technology Park.

References

Adams, J. J., and S. Bachu (2002), Equations of state for basin geofluids: Algorithm review and intercomparison for brines, *Geofluids*, *2*(4), 257–271, doi:10.1046/j.1468-8123.2002.00041.x.

Akbarabadi, M., and M. Piri (2013), Relative permeability hysteresis and capillary trapping characteristics of supercritical CO_2/brine systems: An experimental study at reservoir conditions, *Adv. Water Resour.*, *52*, 190–206, doi:10.1016/j.advwatres.2012.06.014.

Akin, S., and A. R. Kovscek (2003), Computed tomography in petroleum engineering research, *Geol. Soc. Spec. Publ.*, *215*(1), 23–38, doi:10.1144/GSL.SP.2003.215.01.03.

Al-Menhali, A., B. Niu, and S. Krevor (2015), Capillarity and wetting of carbon dioxide and brine during drainage in berea sandstone at reservoir conditions, *Water Resour. Res.*, *51*, 7895–7914, doi:10.1002/2015WR016947.

Andrew, M., B. Bijeljic, and M. J. Blunt (2014), Pore-scale imaging of trapped supercritical carbon dioxide in sandstones and carbonates, *Int. J. Greenhouse Gas Control*, *22*, 1–14, doi:10.1016/j.ijggc.2013.12.018.

Bachu, S., and D. B. Bennion (2008), Effects of in-situ conditions on relative permeability characteristics of CO_2-brine systems, *Environ. Geol.*, *54*(8), 1707–1722, doi:10.1007/s00254-007-0946-9.

Barker, J. W., and P. Dupouy (1999), An analysis of dynamic pseudo-relative permeability methods for oil-water flows, *Pet. Geosci.*, *5*(4), 385–394, doi:10.1144/petgeo.5.4.385.

Bennion, D. B., and S. Bachu (2005), Relative permeability characteristics for supercritical CO2 displacing water in a variety of potential sequestration zones, paper presented at SPE Annual Technical Conference and Exhibition, Soc. of Pet. Eng., Dallas, Tex., 9–12 Oct.

Bennion, D. B., and S. Bachu (2006a), Dependence on temperature, pressure, and salinity of the IFT and relative permeability displacement characteristics of CO_2 injected in deep saline aquifers, paper presented at SPE Annual Technical Conference and Exhibition, Soc. of Pet. Eng., San Antonio, Tex., 24–27 Sept.

Bennion, D. B., and S. Bachu (2006b), The impact of interfacial tension and pore size distribution/capillary pressure character on CO_2 relative permeability at reservoir conditions in CO_2-brine systems, paper presented at SPE/DOE Symposium on Improved Oil Recovery, Soc. of Pet. Eng., Tulsa, Okla., 22–26 April.

Bennion, D. B., and S. Bachu (2008), Drainage and imbibition relative permeability relationships for supercritical CO_2/brine and H_2S/brine systems in intergranular sandstone, carbonate, shale, and anhydrite rocks, *SPE Reservoir Eval. Eng.*, *11*(3), 487–496, doi:10.2118/99326-PA.

Benson, S., R. Pini, C. Reynolds, and S. Krevor (2013), *Relative Permeability Analysis to Describe Multi-Phase Flow in CO2 Storage Reservoirs*, Global CCS Inst., Targeted Report no. 2. [Available at http://www.globalccsinstitute.com/publications/relative-permeability-analysis-describe-multi-phase-flow-co2-storage-reservoirs.]

Berg, S., S. Oedai, and H. Ott (2013), Displacement and mass transfer between saturated and unsaturated CO_2-brine systems in sandstone, *Int. J. Greenhouse Gas Control*, *12*, 478–492, doi:10.1016/j.ijggc.2011.04.005.

Cavanagh, A. J. (2013), Benchmark calibration and prediction of the Sleipner CO_2 plume from 2006 to 2011, *Energy Procedia*, *37*, 3529–3545, doi:10.1016/j.egypro.2013.06.246.

Cavanagh, A. J., and B. Nazarian (2014), A new and extended Sleipner Benchmark model for CO_2 storage simulations in the Utsira formation, *Energy Procedia*, *63*, 2831–2835, doi:10.1016/j.egypro.2014.11.305.

Chadwick, R. A., G. A. Williams, J. D. O. Williams, and D. J. Noy (2012), Measuring pressure performance of a large saline aquifer during industrial-scale CO_2 injection: The Utsira Sand, Norwegian North Sea, *Int. J. Greenhouse Gas Control*, *10*, 374–388, doi:10.1016/j.ijggc.2012.06.022.

Corbett, P. W. M., P. S. Ringrose, J. L. Jensen, and K. S. Sorbie (1992), Laminated clastic reservoirs: The interplay of capillary pressure and sedimentary architecture, paper SPE 24699 presented at SPE Annual Technical Conference and Exhibition, Soc. of Pet. Eng., Washington, D. C., 4–7 Oct.

Dake, L. P. (1983), *Fundamentals of Reservoir Engineering*, Elsevier, Amsterdam, Netherlands.

Egermann, P., and R. Lenormand (2005), A new methodology to evaluate the impact of localized heterogeneity on petrophysical parameters (*kr*, *Pc*) applied to carbonate rocks, *Petrophysics*, *46*(5), 335–345.

Egermann, P., C. A. Chalbaud, J. Duquerroix, and Y. Le Gallo (2006), An integrated approach to parameterize reservoir models for CO_2 injection in aquifers, paper SPE 102308 presented at SPE Annual Technical Conference and Exhibition, Soc. of Pet. Eng., San Antonio, Tex., 24–27 Sept.

Fenghour, A., W. A. Wakeham, and V. Vesovic (1998), The viscosity of carbon dioxide, *J. Phys. Chem. Ref. Data*, *27*(1), 31–44, doi:10.1063/1.556013.

Flett, M., J. Brantjes, R. Gurton, J. McKenna, T. Tankersley, and M. Trupp (2009), Subsurface development of CO_2 disposal for the Gorgon Project, *Energy Procedia*, *1*(1), 3031–3038, doi:10.1016/j.egypro.2009.02.081.

Gupta, R., and D. Maloney (2015), Applications of the intercept method to correct steady-state relative permeability for capillary end-effects, paper SCA2015-001 presented at International Symposium of the Society of Core Analysts, Soc. of Core Anal., St. John's, Newfoundland and Labrador, Canada, 16–21 Aug.

Honarpour, M. M., A. S. Cullick, N. Saad, and N. V. Humphreys (1995), Effect of rock heterogeneity on relative permeability: Implications for scale-up, *J. Pet. Technol.*, *47*(11), 980–986, doi:10.2118/29311-PA.

Hovorka, S. D., et al. (2006), Measuring permanence of CO_2 storage in saline formations: The Frio experiment, *Environ. Geosci.*, *13*(2), 105–121, doi:10.1306/eg.11210505011.

Jonoud, S., and M. D. Jackson (2008), New criteria for the validity of steady-state upscaling, *Transp. Porous Media*, *71*(1), 53–73, doi:10.1007/s11242-007-9111-x.

Kestin, J., H. E. Khalifa, and R. J. Correia (1981), Tables of the dynamic and kinematic viscosity of aqueous NaCl solutions in the temperature range 20–150 C and the pressure range 0.1–35 MPa, *J. Phys. Chem. Ref. Data*, *10*(1), 71–88, doi:10.1063/1.555641.

Kogure, T., O. Nishizawa, S. Chiyonobu, Y. Yazaki, S. Shibatani, and Z. Xue (2013), Effect of sub-core scale heterogeneity on relative permeability curves of porous sandstone in a water-supercritical CO_2 system, *Energy Procedia*, *37*, 4491–4498, doi:10.1016/j.egypro.2013.06.354.

Kong, X., M. Delshad, and M. F. Wheeler (2015), History matching heterogeneous coreflood of CO_2/brine by use of compositional reservoir simulator and geostatistical approach, *SPE J.*, *20*(2), 267–276, doi:10.2118/163625-PA.

Krause, M. H., and S. M. Benson (2015), Accurate determination of charcteristic relative permeability curves, *Adv. Water Resour.*, *83*, 376–388, doi:10.1016/j.advwatres.2015.07.009.

Krause, M. H., S. Krevor, and S. M. Benson (2013), A procedure for the accurate determination of sub-core scale permeability distributions with error quantification, *Transp. Porous Media*, *98*(3), 565–588, doi:10.1007/s11242-013-0161-y.

Krevor, S., R. Pini, L. Zuo, and S. M. Benson (2012), Relative permeability and trapping of CO_2 and water in sandstone rocks at reservoir conditions, *Water Resour. Res.*, *48*, W02532, doi:10.1029/2011WR010859.

Krevor, S., M. J. Blunt, S. M. Benson, C. H. Pentland, C. Reynolds, A. Al-Menhali, and B. Niu (2015), Capillary trapping for geologic carbon dioxide storage—From pore scale physics to field scale implications, *Int. J. Greenhouse Gas Control*, *40*, 221–237, doi:10.1016/j.ijggc.2015.04.006.

Kuo, C. W., and S. M. Benson (2013), Analytical study of effects of flow rate, capillarity, and gravity on CO/brine multiphase-flow system in horizontal corefloods, *SPE J.*, *18*(4), 708–720, doi:10.2118/153954-PA.

Kyte, J. R., and D. W. Berry (1975), New pseudo functions to control numerical dispersion, *Soc. Pet. Eng. J.*, *15*(4), 269–276, doi:10.2118/5105-PA.

Levine, J. S., D. S. Goldberg, K. S. Lackner, J. M. Matter, M. G. Supp, and T. S. Ramakrishnan (2014), Relative permeability experiments of carbon dioxide displacing brine and their implications for carbon sequestration, *Environ. Sci. Technol.*, *48*(1), 811–818, doi:10.1021/es401549e.

Li, X., E. Boek, G. C. Maitland, and J. P. M. Trusler (2012), Interfacial tension of (brines+ CO_2):(0.864 NaCl+ 0.136 KCl) at temperatures between (298 and 448) K, pressures between (2 and 50) MPa, and total molalities of (1 to 5) mol·kg^{-1}, *J. Chem. Eng. Data*, *57*(4), 1078–1088, doi:10.1021/je201062r.

Manceau, J. C., J. Ma, R. Li, P. Audigane, P. X. Jiang, R. N. Xu, J. Tremosa, and C. Lerouge (2015), Two-phase flow properties of a sandstone rock for the CO_2/water system: Core-flooding experiments, and focus on impacts of mineralogical changes, *Water Resour. Res.*, *51*, 2885–2900, doi:10.1002/2014WR015725.

Muskat, M., and M. W. Meres (1936), The flow of heterogeneous fluids through porous media, *J. Appl. Phys.*, *7*(9), 346–363, doi:10.1063/1.1745403.

Niu, B., A. Al-Menhali, and S. C. Krevor (2015), The impact of reservoir conditions on the residual trapping of carbon dioxide in berea sandstone, *Water Resour. Res.*, *51*, 2009–2029, doi:10.1002/2014WR016441.

Nordbotten, J. M., M. A. Celia, and S. Bachu (2005), Injection and storage of CO_2 in deep saline aquifers: Analytical solution for CO_2 plume evolution during injection, *Transp. Porous Media*, *58*(3), 339–360, doi:10.1007/s11242-004-0670-9.

Pentland, C. H., R. El-Maghraby, S. Iglauer, and M. J. Blunt (2011), Measurements of the capillary trapping of super-critical carbon dioxide in Berea sandstone, *Geophys. Res. Lett.*, *38*, L06401, doi:10.1029/2011GL046683.

Perrin, J. C., and S. Benson (2010), An experimental study on the influence of sub-core scale heterogeneities on CO_2 distribution in reservoir rocks, *Transp. Porous Media*, *82*(1), 93–109, doi:10.1007/s11242-009-9426-x.

Phillips, S. L., A. Igbene, J. A. Fair, H. Ozbek, and M. Tavana (1981), A technical databook for geothermal energy utilization, *Rep. 12810*, Lawrence Berkeley Natl. Lab., Calif. [Available at http://escholarship.org/uc/item/5wg167jq.]

Pickup, G. E., and K. D. Stephen (2000), An assessment of steady-state scale-up for small-scale geological models, *Pet. Geosci.*, *6*(3), 203–210, doi:10.1144/petgeo.6.3.203.

Pini, R., and S. M. Benson (2013), Simultaneous determination of capillary pressure and relative permeability curves from core-flooding experiments with various fluid pairs, *Water Resour. Res.*, *49*, 3516–3530, doi:10.1002/wrcr.20274.

Pini, R., S. C. M. Krevor, and S. M. Benson (2012), Capillary pressure and heterogeneity for the CO_2/water system in sandstone rocks at reservoir conditions, *Adv. Water Resour.*, *38*, 48–59, doi:10.1016/j.advwatres.2011.12.007.

Pope, G. A. (1980), The application of fractional flow theory to enhanced oil recovery, *SPEJ Soc. Pet. Eng. J.*, *20*(3), 191–205, doi:10.2118/7660-PA.

Rabinovich, A., K. Itthisawatpan, and L. J. Durlofsky (2015), Upscaling of CO_2 injection into brine with capillary heterogeneity effects, *J. Pet. Sci. Eng.*, *134*, 60–75, doi:10.1016/j.petrol.2015.07.021.

Rapoport, L. A. (1955), Scaling laws for use in design and operation of water-oil flow models, *Pet. Trans.*, *204*, 143–150.

Ringrose, P. S., K. S. Sorbie, P. W. M. Corbett, and J. L. Jensen (1993), Immiscible flow behaviour in laminated and cross-bedded sandstones, *J. Pet. Sci. Eng.*, *9*(2), 103–124, doi:10.1016/0920-4105(93)90071-L.

Rogers, J. D., and R. B. Grigg (2000), A literature analysis of the WAG injectivity abnormalities in the CO_2 process, paper SPE 59329-MS presented at SPE/DOE Improved Oil Recovery Symposium, Soc. of Pet. Eng., Tulsa, Okla., 3–5 April.

Ruprecht, C., R. Pini, R. Falta, S. Benson, and L. Murdoch (2014), Hysteretic trapping and relative permeability of CO_2 in sandstone at reservoir conditions, *Int. J. Greenhouse Gas Control*, *27*, 15–27, doi:10.1016/j.ijggc.2014.05.003.

Shi, J. Q., Z. Xue, and S. Durucan (2011), Supercritical CO_2 core flooding and imbibition in Tako sandstone: Influence of sub-core scale heterogeneity, *Int. J. Greenhouse Gas Control*, *5*(1), 75–87, doi:10.1016/j.ijggc.2010.07.003.

Shook, M., D. Li, and L. W. Lake (1992), Scaling immiscible flow through permeable media by inspectional analysis, *In Situ*, *16*(4), 311–349.

Sorbie, K. S., L. J. Roberts, and R. W. S. Foulser (1982), *Polymer flooding calculations for highly stratified brent sands in the north sea*, presented at the 2nd European Symposium on Enhanced Oil Recovery, Paris, 8–10 November.

Taber, J. J. (1969), Dynamic and static forces required to remove a discontinuous oil phase from porous media containing both oil and water, *SPE J.*, *9*(1), 3–12, doi:10.2118/2098-PA.

Virnovsky, G. A., H. A. Friis, and A. Lohne (2004), A steady-state upscaling approach for immiscible two-phase flow, *Transp. Porous Media*, *54*(2), 167–192, doi:10.1023/A:1026363132351.

Wei, N., M. Gill, D. Crandall, D. McIntyre, Y. Wang, K. Bruner, X. Li, and G. Bromhal (2014), CO_2 flooding properties of Liujiagou sandstone: Influence of sub-core scale structure heterogeneity, *Greenhouse Gases: Sci. Technol.*, *4*(3), 400–418, doi:10.1002/ghg.1407.

Yokoyama, Y., and L. W. Lake (1981), The effects of capillary pressure on immiscible displacements in stratified porous media, paper presented at SPE 10109 SPE Annual Technical Conference and Exhibition, Soc. of Pet. Eng., San Antonio, Tex., 5–7 Oct.

Zhang, Y., T. Kogure, S. Chiyonobu, X. Lei, and Z. Xue (2013), Influence of heterogeneity on relative permeability for CO_2/brine: CT observations and numerical modeling, *Energy Procedia*, *37*, 4647–4654, doi:10.1016/j.egypro.2013.07.241.

Zhang, Y., O. Nishizawa, T. Kiyama, S. Chiyonobu, and Z. Xue (2014), Flow behaviour of supercritical CO_2 and brine in Berea sandstone during drainage and imbibition revealed by medical X-ray CT images, *Geophys. J. Int.*, *197*(3), 1789–1807, doi:10.1093/gji/ggu089.

Zhou, D., F. J. Fayers, and F. M. Orr Jr. (1997), Scaling of multiphase flow in simple heterogeneous porous media, *SPE Reservoir Eng.*, *12*(3), 173–178, doi:10.2118/27833-PA.